A Chemical Pathway Perspective on the Kinetics of Low-Temperature Ignition of Propane

Shirong Bai, Michael J. Davis, Raghu Sivaramakrishnan and Rex T. Skodje*a

- a) Department of Chemistry and Biochemistry, University of Colorado, Boulder, Colorado, 80309
 - b) Chemical Sciences and Engineering Division, Argonne National Laboratory, Argonne IL 60439

Abstract

The chemistry of low-temperature ignition in propane/air mixtures is analyzed using a recently developed pathway representation of the chemical kinetics. The "Sum Over Histories Representation" allows time-dependent kinetic observables to be computed using an expansion over global chemical pathways that follow chemical moieties as they move through a complex reaction network. This methodology assigns probabilities to complete chemical pathways through which specific intermediate or product species are generated. The growth of the radical pool during the ignition process is analyzed by enumerating chemical pathways that constitute catalytic cycles, in particular the catalyzed production of the highly reactive OH-radical. In addition to the well-known reaction route followed in low-temperature ignition of hydrocarbons which involves the QOOH and keto-hydroperoxide species, we have explicitly identified several other cycles that are responsible for most of the remaining OH-production.

I. Introduction

Autoignition of hydrocarbons is a critical process underlying engine performance and has been the focus of intense efforts both in the laboratory and using chemical modeling [1-3]. The ignition properties of a given fuel can, in principle, be predicted from a kinetic simulation given a well-defined mechanism [4]. It is well appreciated that for most fuels there is a great deal of uncertainty in the chemical models that are employed in these simulations. Consequently, for both the ignition problem and more general analysis of chemical combustion, a variety of schemes have been developed to identify and improve the rate expressions for key reaction steps that have high degrees of uncertainty or likely error. In this regard, we mention the use of sensitivity analysis [5-10], uncertainty quantification [11, 12] and various updating procedures within automatic mechanism generation methods. In a similar vein, we note the program of mechanism reduction (or simplification) in which large mechanisms are reduced using insights into the key chemistry of the mechanism [13-15]. In almost all approaches to model improvement, the refinement of the chemical mechanism proceeds through a robust interplay between model development and kinetic simulation and prediction. To make effective use of any of these mechanism improvement strategies, it is important to have a physical understanding of the essential chemistry underlying the ignition process for the fuel in question. In this work, we shall describe and implement a new approach to kinetic simulation that leads to new insight into the workings of a realistic autoignition problem.

In traditional chemical modeling, observables such as the species concentrations are obtained by solving differential equations (ODE's)

$$\frac{dX}{dt} = F(X) \tag{1}$$

where X(t) is the species concentration vector and F(X) is the vector of species sources and sinks composed from the elementary steps within the full mechanism. It is a "local" method in the sense that the growth of concentrations results from instantaneous fluxes of single reaction steps into and out of the various species. Recently, we have suggested a "global" strategy based on complete chemical pathways involving multiple species and reactions that carry a chemical moiety from a reagent to a product or intermediate over a finite period of time [16-20]. The chemical pathway tracks a chemical moiety through species-space as it jumps from species to species due to the

action of elementary chemical reactions. This quantitative theory, which we called the Sum over Histories Representation (or SOHR), allows the time-dependent value of any kinetic observable to be expressed using a linear combination of pathway probabilities. This approach bears similarity to various other methods that interpret kinetics using symbolic or graph theoretic representations [21, 22]. For example, the species concentration of S_i , $X_i(t)$, is

$$X_i(t) = \sum_i c_i P_i(t) \tag{2}$$

In eq. (2), j is a generalized index labeling chemical pathways, c_j are trivial coefficients depending on the initial concentrations and reaction stoichiometry, and $P_j(t)$ the pathway probabilities for a chemical moiety to follow path j from reagents to the species S_i . Each chemical pathway has a unique probability that can be computed exactly. Equation 2 is a representation of the chemical propagator $T(t_0,t)$ in terms of chemical pathways, where $X(t) = T(t_0,t) \cdot X(t_0)$. Since the theory is formulated in terms of probabilities, the expression is linear in the initial concentration $X(t_0)$ even though the kinetics may be nonlinear. In a recent simulation [17, 20], we demonstrated that the concentrations of all species in a realistic hydrogen combustion model could be computed to within 1% using a small number of pathways that deliver a tagged reagent atom to product and intermediate species.

The SOHR method can be used in two distinct ways: 1) as a method of chemical analysis in which the chemical kinetics is first solved using a conventional ordinary differential equation (ODE) solver and then the chemical pathways are identified and their probabilities computed; and 2) as a predictive method in which the pathways and probabilities are computed iteratively from the mechanism so the ODE's need never be solved [20]. For the present work, we shall focus on the use of SOHR for an analysis of how the ignition process occurs. In particular, by decomposing the kinetics into individual chemical pathways with well-defined probabilities we can obtain a mechanistic and improvable picture of the ignition process.

In this work we analyze the low-temperature ignition kinetics of propane/air using the chemical pathway method. We shall make use of the model proposed by Goldsmith *et al.* and Merchant *et al.* [23, 24] consisting of 110 species and 631 elementary reactions. The quantitative description of the radical pool underlying the ignition phenomenon is well studied for many classes of fuels and reflects the interplay of chain branching, propagation, and termination reactions. As recently summarized by Zádor *et al.* [25] a commonly held scenario [26-28] for the low

temperature ignition of alkane hydrocarbons involves passage through a common set of intermediate species that leads to net chain branching and ignition. Briefly, the hydrocarbon (RH) is attacked by a radical yielding an alkyl radical (R) which quickly attaches to an O₂ molecules to form the alkylperoxy radical (RO₂). An internal H-atom transfer occurs isomerizing RO₂ into a hydroperoxyalkyl radical (QOOH) to which another O₂ can attach yielding the hydroperoxyalkylperoxy radical O₂QOOH. The O₂QOOH undergoes another internal H-atom transfer to form HOOQ'OOH where the radical site has migrated to the carbon atom. This species very quickly decomposes into OH and a ketohydroperoxide OQ'OOH. The relatively long-lived OQ'OOH species thermally decomposes yielding OH+OQ'O. The alkoxy radical, OQ'O, undergoes subsequent reactions that produce one further OH radical and various other species such as aldehydes. This conjectured primary route to chain branching, of course, represents just a small subset of reaction steps that are imbedded within the much larger full mechanism. The secondary chemistry induced by competing branching routes and reactions of combustion byproducts may either enhance or inhibit the overall chain branching character of the mixture [29, 30].

As illustrated by the recent work of Merchant et al. [24], we can view the primary reaction route outlined above as an auto-catalytic cycle. In this cycle, the OH-radical serves as the catalytic center (or carrier) which is consumed to initiate reaction with propane, but is multiply regenerated by subsequent reaction steps. Since the OH species is the most reactive and important radical, the growth of OH then guides the growth of the radical pool prior to ignition. As shown in Fig. 1, the OH-radical is consumed as it attacks the propane fuel but is also liberated at various points of the cycle. In an ideal cycle there would be three OH's produced and one OH consumed, resulting in a net production of two OH's. Defining γ to be the net number of OH-radicals generated per cycle, one has $\gamma=2$ for the ideal cycle (i.e. three OH's produced and one consumed), implying a chain branching autocatalytic process. However, the true kinetics of the full mechanism will yield deviations from this idealization. As noted by Merchant et al. [24], one important loss mechanism for the cycle involves branching at the initiation step, OH+C₃H₈→H₂O+C₃H₇ where the H-atom abstraction reaction yields the n-propyl (nR) and i-propyl (iR) radicals in roughly equal proportions. While the nR follows the primary reaction pathway sketched in Fig. 1, the iR generates the isopropyl peroxy radical (iRO₂) which does not efficiently form QOOH and decays mostly to the much less reactive radical HO₂. Another loss mechanism along the cycle is the elimination

reaction nRO₂ \rightarrow HO₂+propene that competes with the production of QOOH. Merchant *et al.* [24]²⁴

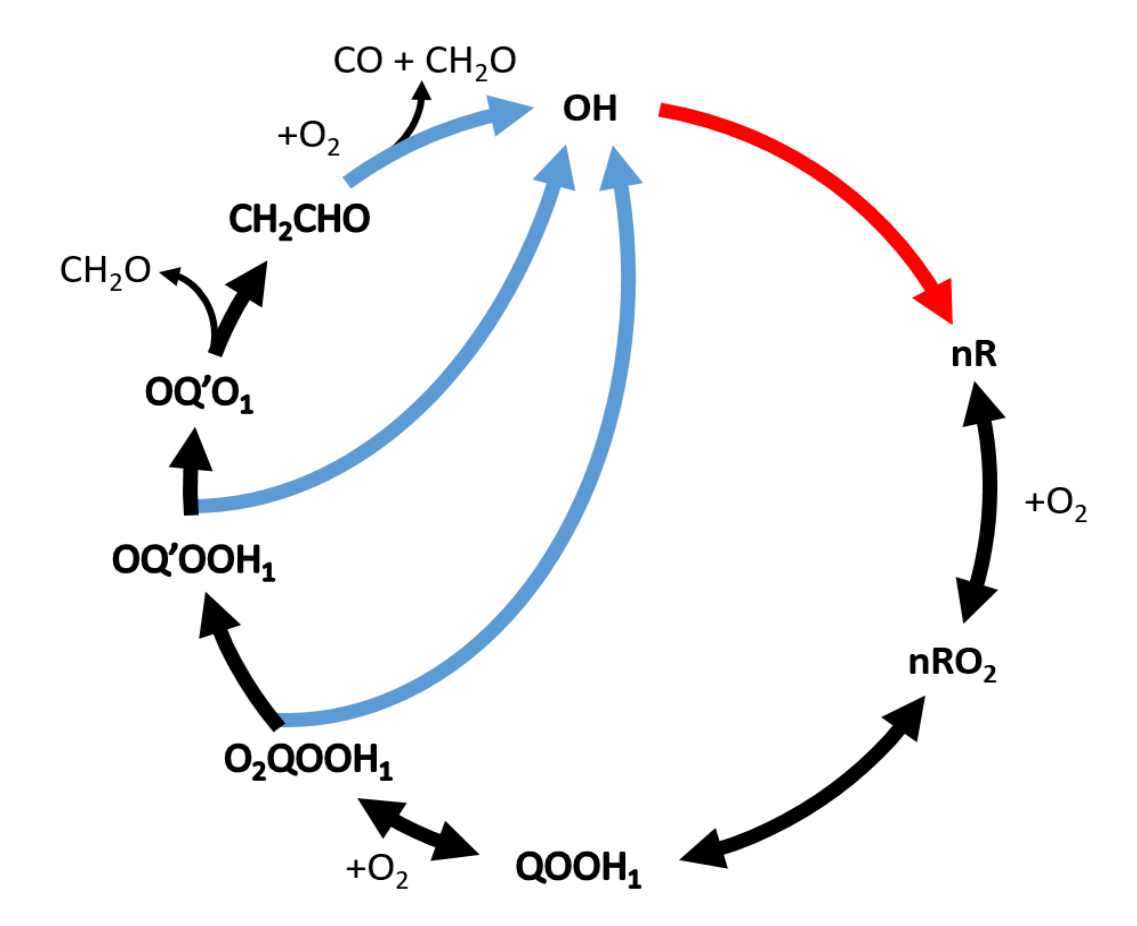


Fig. 1 A schematic diagram showing the primary auto-catalytic cycle for propane ignition for the OH-catalytic center. In the center circle the propane fuel molecule undergoes a sequence of reactions passing through the species RH, nR, nRO₂, QOOH, O₂QOOH, OQ'OOH, OQ'O, CH₂CHO, and finally CO and CH₂O products. One OH is assumed to be consumed to initiate the sequence and up to three OH's are liberated by subsequent reactions.

found that when the net OH production along the primary cycle was evaluated from kinetic simulations, a number of features of the early stages of ignition could be predicted. Complicating

this simple scheme are effects of a large number of secondary processes. These include minor reaction channels and reactions involving the combustion products with each other. One goal of this work is to explicitly map out the kinetics of this secondary chemistry using an existing propane model. It is hoped that insights developed from this work will assist in the improvement of the mechanism.

Low-temperature ignition of propane, like that for many other fuels [31], is a two stage process. In two stage ignition, one observes a pronounced pause in the growth of the radical pool, and hence in the temperature rise, before the final "full" ignition occurs. The distinct ignition stages reflect different chemistry brought on by the evolution of the chemical composition of the system as well as changes in the temperature and pressure. The existence of a first (failed) ignition threshold is known to be attributable to changes in the chemistry that lead to inhibition of chain branching. Understanding the origin of boundaries separating slow combustion from explosive chemistry was an impressive early success of gas phase chemical kinetics [32, 33, 34]. Simple models were developed that could account for the transition between these distinct kinetic regimes based on the balance between the creation and annihilation of radical centers responsible for chain branching, propagation, and termination. These models could account quite well for the explosion thresholds in a simple fuel such as hydrogen. For complicated fuels, the prediction of kinetic phase boundaries is more challenging. Therefore, it is quite interesting that aspects of the propane/air system can apparently be explained in terms of the efficiency of a single catalytic cycle of the OHradical. Merchant et al. [24] found that a simple kinetic model could describe the first stage ignition threshold as a transition to slow combustion. One issue of interest in this work is whether we can account more fully for the ignition chemistry by elaborating any additional catalytic cycles that may exist for propane.

In Sec. II, we introduce the theoretical methodology used to analyze the propane ignition kinetics using the pathway approach. The basic SOHR methodology, presented previously, is reviewed in II.A. In II.B, we introduce the concept of merged chemical pathways that are obtained by summing over paths that link pairs of species by various elementary reactions. In Sec. II.C an approach is presented to compute the time-dependent catalytic efficiency of a cycle. In Sec. II.D the notion of a chattering group is introduced. The chattering group (CG) is a set of species that rapidly interconverts but is relatively weakly chemically coupled to species outside of the group;

it is analogous to a group of species that lie in quasi-steady state. This notion is closely related to that of a lumped group of species extensively discussed elsewhere [10, 35, 36, 37] and is also very reminiscent of the species family method employed in atmospheric chemistry[38]. Section III briefly reviews the propane combustion model we employ. In Sec. IV, the convergence of the SOHR pathway expansion is demonstrated numerically by comparing to the results of traditional kinetic modeling. In Sec. V, the CG's uncovered for low temperature propane ignition are presented and it is shown how their relative concentrations compare with the predictions of a steady state approximation. In Sec. VI, the ignition properties of propane/air are analyzed using the autocatalytic model of OH production. The efficiency of the primary cycle is computed exactly and is found to lie within about 25% of the prediction of a simple steady state approximation. Several secondary cycles are identified and quantified in which the OH production occurs through mechanisms distinct from the conventional primary cycle. Sec.VII presents a conclusion which summarizes the paper and discusses in more detail some of the important secondary reactions identified by the SOHR method.

II. Pathway Representation

In this section, we briefly review the SOHR method and discuss several adaptations necessary to treat propane ignition and more complicated kinetic mechanisms in general. Although it is possible to generalize the treatment to spatially inhomogeneous and nonstatistical processes, we shall assume that the kinetics is accurately described by the conventional homogeneous rate equations in the concentrations $\{X_i(t)\}_{i=1}^N$ plus the thermodynamic variables.

A. Sum Over Histories Representation

In the SOHR method, the time-development of a homogeneous reactive system consisting of N distinct species coupled by M elementary reactions is represented in terms of chemical pathways that transfer chemical moieties from an initial set of species, $\{S_0^i\}$, to a final set of species $\{S_f^i\}$. While the term "reaction pathway" is widely used in chemical science, there are a variety of definitions employed [39-49]. To use the SOHR model, it is important to have a specific definition that can serve as the basis for a quantitative description of the kinetics. We adopted a graph theoretic approach based on an "atom-following" algorithm that allows for a complete enumeration of the relevant paths on a chemical graph. There, each chemically distinct atom (or

indestructible chemical moiety) is tagged and followed as it hops from species to species through the action of the elementary reactions and hence defines adjacency on the graph[50]. If the reactions, $\{R_j\}_{j=1}^M$ are viewed as a sequence of random events occurring with transition probability per unit time of $\rho_j(t_j)$ then a time resolved n-step pathway can be expressed as S_0 $\xrightarrow{R_1(t_1)} S_1 \xrightarrow{R_2(t_2)} S_2 \dots \xrightarrow{R_n(t_n)} S_n$; hence the path is specified by the reaction sequence, the species in which the tagged atom resides, and times at which the reactions occur. The reactions obey time ordering, i.e. $t_n \ge t_{n-1} \ge \cdots t_1$ but otherwise occur randomly over a range of times. The key to a quantitative pathway description of the kinetics is to develop an efficient method to compute the probability associated with each pathway. We define $P_j(t_0,t_f)$ to be the probability of a tagged atom originating in species S_0 at time t_0 and lying in species S_n at time t_f assuming it follows a specific path labeled by j. We have shown that the $P_j(t_0,t_f)$ is given by the time-ordered integral [17]

$$P_{j}(t_{0}, t_{f}) = (-1)^{n} \int_{t_{0}}^{t_{f}} dt_{n} \int_{t_{0}}^{t_{n}} dt_{n-1} \dots \int_{t_{0}}^{t_{2}} dt_{1} \prod_{i=1}^{n} \left(\frac{d\mathcal{P}_{i-1}(t_{i-1}, t_{i})}{dt_{i}} \Gamma_{i-1}(t_{i}) \right) \mathcal{P}_{n}(t_{n}, t_{f})$$
(3)

which can be evaluated using the Monte Carlo representation

$$P_{j}(t_{0}, t_{f}) = \frac{1}{L} \sum_{q=1}^{L} \left(\mathcal{P}_{n}(t_{n}^{q}, t_{f}) \prod_{k=1}^{n} \left(\Gamma_{k-1}(t_{k}^{q}) \left(1 - \mathcal{P}_{min}^{k-1}(t_{k}^{q}) \right) \right) \right)$$
(4)

with L sufficiently large. The species survival probability $\mathcal{F}_i(t_a, t_b)$ is the probability that a molecule of S_i present at time t_a will survive to a time t_b ; it can be obtained easily from the time-dependent decay rate of S_i due to its elementary sink reactions $\{R_l^{i,sink}\}$. If the elementary rates for the sink reactions are $\{\omega_l^i(t)\}$ then

$$\mathcal{F}_{i}(t_{a}, t_{b}) = exp\left(-\int_{t_{a}}^{t_{b} sinks \ of \ i} \omega_{l}^{i}(t) / [X_{i}]dt\right)$$
 (5)

where $\omega_l^i(t)/[X_i]$ is the decay rate per molecule of S_i via reaction R_l . The time-dependent reaction branching ratio $\Gamma_i(t)$ is the fraction of molecules of type S_i that decay according to the "proper" reaction " R_J " for a given step along the reaction pathway j of interest (the indices j and J are dropped from $\Gamma_i(t)$ dropped for brevity). It is given by

$$\Gamma_i(t) = \frac{\omega_J^i(t)}{\sum_l \omega_l^i(t)} \tag{6}$$

where J comes from the specification of the chemical pathway. We define \mathcal{P}_{min}^k to be the smallest value achievable by the survival probability of the k^{th} species which occurs at the endpoint of the allowed time range. Thus, to evaluate eq. (4), L strings of n-random numbers are chosen to uniformly sample \mathcal{P}_i and are labeled by the index q. The survival probabilities $\mathcal{P}_k(t_k^q, t_f)$ are randomly selected and the corresponding reaction times are found by simple interpolation. All quantities required in eq. (4) can be easily obtained from the kinetic trajectory and the elementary rate laws.

In the interpretive SOHR method, we account for kinetic observables in terms of the pathway contributions, even though the kinetic trajectory X(t) is already known. We have shown [17, 19] that the concentrations themselves are given by a sum over the paths j

$$[X_i(t)] = \sum_j c_j P_j(t_0, t) [X_{r(j)}(t_0)] \qquad i = 1, ..., N$$
 (7)

where c_j are trivial coefficients obtained from the reaction stoichiometry and $[X_{r(j)}(t_0)]$ are the concentrations of all species containing the tagged atom at time t_0 . The sum is converged by adding pathways until $[X_i(t)]$ achieves a value sufficiently close to the known result.

In the predictive SOHR method, we eliminate the need for the reference trajectory altogether and produce a "stand alone" theory which can predict the time evolution of the kinetics without the need to solve the conventional ODE's. We have recently shown that eqs. (3) and (7) can be iteratively solved by using an initial guess for the concentration profiles, X(t) [20]. The initial guess could often be the trivial choice of constant concentrations. The efficiency of the computation was greatly enhanced using a sector-by-sector propagation method in which the pathways were defined in a set of intervals spanning the time range [20²⁰].

B. Enumerating and Merging Pathways

Much of the SOHR algorithm involves enumerating the chemical pathways connecting the initial species to the intermediate and product species. While for simple problems chemical insight will reveal the relevant pathways, most complicated mechanisms require a more automated

approach. We have found that a statistical sampling method based on the "stochastic simulation algorithm" of Gillespie is often quite useful [51, 52]. There, given moieties are propagated through the chemical network using a kinetic Monte Carlo simulation; the pathways followed by the moieties are recorded and added to a running list. The pathway probability is screened using eq. (4) with small L and it is retained if the probability is sufficiently high. The chemical pathways, and their probabilities, obtained in this way are fully delineated and unique in that the species and elementary reaction are specified for each reaction step.

While the atom-following algorithm is in principle a foolproof method, it is also true that it can lead to an explosion in the number of chemical paths with relatively little gain in insight. Consider a family of two step pathways consisting of a sequence of two H-atom abstractions from a species XH_2 by a free radical R, $XH_2 \xrightarrow{+R} XH \xrightarrow{+R} XI$. If there are M different free radical species, then there are M^2 distinct pathways of this type. Clearly a "merged reaction" model consisting of a single path that has lumped together all the radical reactions capable of H-atom abstraction conveys nearly as much information as do the M^2 paths. We may compute the associated probability using a single evaluation of eq. (3) where the individual branching ratio $\Gamma_i(t)$ is now replaced by the sum of the branching ratios for all the included abstraction reactions experienced by S_i at time t. In the limit where all possible reactions that converge S_i to S_{i+1} are contracted, the reaction merged pathway can be represented as a sequence of species.

C. Catalytic Cycles

To understand and predict the behavior of the ignition threshold for the propane fuel, it is useful to consider the traditional model of chain branching reaction networks. The steady state picture of chain branching reactions, in which a small radical source term is amplified, is well-known. As discussed by Hinshelwood [33] and Semenoff [3434]³⁴, the kinetics is modeled by following a radical center "X" which initiates reaction(s) of a reagent "R", present in great excess, which is converted to product(s) "P" through a number of steps and is regenerated in the course of the catalytic cycle. The first step of the cycle is X+R, but a possibly different rate limiting step of the cycle is described by the pseudo-first-order rate law k_{eff} [X]. Auto-catalysis is quantified by the parameter γ , which is the net number of radical centers generated/destroyed during one passage through the cycle, and which is usually computed from the instantaneous (snapshot) reaction branching ratios for the branching and termination steps around the cycle. The transition from slow

combustion (γ <0) to chain branching explosion (γ >0) is predicted to lie at the explosion limit of $\gamma = 0$. For $\gamma < 0$ the chain length is $\ell = -1/\gamma$. The steady state picture predicts the exponential growth/decay rate of [X] to be $\sim exp(\gamma k_{eff}t)$. This model assumes the passage around the catalytic cycle is instantaneous in the sense that γ radicals are produced on a time scale rapid compared to any variation of k_{eff} that may result, e.g. from concentration or temperature changes. In reality, the passage around the cycle (and the release of autocatalytic X-radicals) is distributed over a finite range of times. Thus, we can define a quantity $\chi(t, t + \delta)$ which is the number of X-radicals generated during a time window $[t,t+\delta]$ assuming that the cycle is initiated at time t by R+X. If the catalytic chemistry is truly rapid, then $\chi(t, t + \delta)$ quickly approaches its limiting value as δ is increased. If, in contrast, the cycle chemistry is slow then the growth/decay rate of [X(t)] may be poorly described by the snapshot picture. Instead, the catalytic growth of X should be modeled using a related two-point function $\gamma(t, t + \delta) = \alpha(t) \cdot \chi(t, t + \delta) - 1$ where $\alpha(t)$ is the reaction branching ratio of the initiation step, X+R, occurring at time t, with new X's being produced at a rate $d\chi(t, t + \delta)/d\delta \ge 0$; the "-1" is introduced to reflect the consumption of one X-radical to initiate the cycle. The growth rate of X is then obtained from a convolution integral over $\chi(t, t + \delta)$. We may easily calculate $\chi(t, t + \delta)$ from the arrival time distribution at the final (OHproducing) step that yield the co-product Sfinal. We have

$$\chi(t,t+\delta) = \sum_{j}^{pathways} \chi_{j}(t,t+\delta) = \sum_{j}^{pathways} n_{j}\bar{P}_{j}(t,t+\delta)$$
 (8)

where the sum is over all pathways comprising the catalytic cycle and n_j is the number of X-radicals generated at the last step of the path which is typically a positive whole number. The "cumulative pathway probability" $\bar{P}_j(t, t + \delta)$ is obtained by integrating the arrival time distribution for path j, i.e.

$$\bar{P}_{j}(t,t+\delta) = \int_{t}^{t+\delta} \frac{d(P_{j}(t,t')/\mathcal{P}_{final}(t,t'))}{dt} dt'$$
(9)

The need for integration can be avoided by computing the probability by evaluating eq. (4) with the decay rate of the final species along the pathway set to zero (i.e. $\mathcal{P}_{final}(t_a, t_b) = 1$). When

more than one interlocking catalytic cycle is involved in the chain reaction (as it is for OH-production in propane), a somewhat more complicated expression is required for the chain length. In general, we require a separate determination of χ for each catalytic cycle, which need to be combined with separate branching fractions (such as defined above) to determine the overall catalytic efficiency.

D. Chemical Chattering: The Chattering Group

The number of required chemical pathways in the SOHR method can become overwhelmingly large in certain cases when a separation of timescales exists between various reversible reactions. For example, consider the process $A \rightarrow X \leftrightarrow Y \rightarrow B$ where the forward and backward reactions, $X \leftrightarrow Y$, are very rapid, but the formation and decay reactions $A \rightarrow X$ and $Y \rightarrow B$ are very slow. We then typically encounter numerous very long pathways like

$$A \rightarrow X \rightarrow Y \rightarrow X \rightarrow Y \rightarrow X \dots \rightarrow Y \rightarrow B$$

where the reaction "chatters" between X and Y many times before proceeding to products. Thus, the description of the net reaction A→B requires a very large number of chattering pathways of very long lengths. Clearly, the net result of this chattering is the near establishment of a quasiequilibrium distribution of the species X and Y. A much more compact representation of the pathways involves merging X and Y into a single group Z so that the effective reaction pathway is $A \rightarrow Z \rightarrow B$. These CG's may be identified by recurring patterns of species in stochastic pathway simulation, community structure in chemical graphs, or a priori by free energy considerations. After the CG is identified, the "species" Z is assigned a composite non-reaction probability, $\mathcal{P}_Z(t_a, t_b)$, and branching ratio, $\Gamma_Z(t)$ into various products, i.e. Z \rightarrow product. The SOHR method does not require that components of Z actually obey a steady state distribution. In the example above, the instantaneous decay rate of Z, ω_z , is obtained from the sinks of X and Y ω_Z = $\sum_{i}^{X-sink} \omega_{i}^{X} + \sum_{i}^{Y-sink} \omega_{i}^{Y}$ where the interconversion reactions X \leftrightarrow Y have been dropped from the list of possible sink reactions. The branching ratios are obtained using the formula $\Gamma_i(t)$ = $\omega_I^i(t)/\sum_l \omega_l^i(t)$ but the branch J is only allowed to connect molecules of the CG to species on the outside of the CG and the summation over l omits the reactions which interconvert the chattering species. More generally, we may find a CG comprised of several species $Z=\{X_i,\}$ $i=1,...N_G$, which interconvert rapidly but decay to the "outside" much more slowly. To compute the pathway

probability for the contracted chattering paths we compute the rates $\omega_l^i(t)$ from the reference trajectory and thus no quasisteady state approximation is invoked. Effectively, the CG approach is a means to automatically sum the infinite number of chattering pathways that occur in the expansion of observables such as $[X_i(t)] = \sum_j c_j P_j(t_0, t) [X_{r(j)}(t_0)]$. Although there are certain subtle distinctions in the precise definition, the CG is quite similar to groups of lumped species that could be identified by means of time scale separation based on the rate equations [10,35,36].

III. Propane Model

The chemistry of propane combustion is modeled using the mechanism developed in refs. [23] and [24]. Many of the essential reaction steps involving the three-carbon containing species are not currently accessible to experiment and have been studied with *ab initio* potential energy surfaces and statistical rate theory. These processes include the key reactions of the primary catalytic cycle envisioned in Fig. 1. [One motivation for the pathway analysis is to predict other key reactions necessary for other catalytic cycles.] The reactions involve two isomers of RO₂ (nRO₂ and iRO₂), three isomers of QOOH (labeled QOOH₁, QOOH₂, and QOOH₃ where the number denotes the location of the radical site), and five isomers of O₂QOOH denoted as well1-well5. After the first OH-fission reaction of O₂QOOH, a set of seven ketohydroperoxide isomers OQ'OOH (denoted as prod1-prod7) are formed. The primary isomers along the chain branching mechanism sketched in Fig. 1 are nR, RO₂, QOOH₁, O₂QOOH₁, prod1, and frag1. The OQ'OOH species can decay into one of four fragments OQ'O. The decay of O₂QOOH into other secondary products involving HO₂ elimination are also modeled in the mechanism. A subset of the 631 reactions comprising the mechanism is presented in Table 1. These reactions are singled out because they will be used as steps in important chemical pathways identified by the SOHR method.

Table 1. Important reactions in the propane/O₂ ignition chemistry.

Reaction Index	Reaction
1	$RH + O_2 \rightarrow nR + HO_2$
2	$RH + O_2 \rightarrow iR + HO_2$
3	$RH + OH \rightarrow nR + H_2O$
4	$RH + OH \rightarrow iR + H_2O$

5	$RH + HO_2 \rightarrow iR + H_2O_2$
6	$iROO \rightarrow O_2 + iR$
7	$O_2QOOH_1 \rightarrow O_2 + QOOH_1$
8	$RH + HO_2 \rightarrow nR + H_2O_2$
9	$O_2 + iR \rightarrow HO_2 + C_3H_6$
10	$nROO \rightarrow O_2 + nR$
11	$O_2QOOH_1 \rightarrow OH + OQ'OOH_1$
12	nROO + RH → nROOH + iR
13	iROO + RH → iROOH + iR
14	iROO + RH → iROOH + nR
15	$HO_2 + HO_2 \rightarrow H_2O_2 + O_2$
16	$iROO \rightarrow HO_2 + C_3H_6$
17	iROOH → iRO + OH
18	$OQ'OOH_1 \rightarrow OQ'O_1 + OH$
19	CH ₃ OO + RH → CH ₃ OOH + iR
20	nROOH → nRO + OH
21	nROO + RH → nROOH + nR
22	$OQ'O_1 \rightarrow vinoxy + CH_2O$
23	iRO → CH ₃ + acetaldehyde
24	$CH_3CH_2OO + RH \rightarrow CH_3CH_2OOH + iR$
25	$nRO \rightarrow C_2H_5 + CH_2O$
26	$CH_3OO + RH \rightarrow CH_3OOH + nR$
27	$vinoxy + O_2 \rightarrow CH_2O + CO + OH$
28	$O_2 + nR \rightarrow HO_2 + C_3H_6$
29	$CH_3CH_2OO + RH \rightarrow CH_3CH_2OOH + nR$
30	$CH_3OO(+M) \rightarrow CH_3 + O_2(+M)$
31	$CH_3CH_2OO \rightarrow C_2H_5 + O_2$
32	$nROO \rightarrow HO_2 + C_3H_6$
33	$QOOH_1 \rightarrow O_2 + nR$
34	$C_2H_5 + O_2 \rightarrow C_2H_4 + HO_2$
35	$iROO + HO_2 \rightarrow iROOH + O_2$
36	$O_2 + QOOH_1 \rightarrow OH + OH + OQ'O_1$
37	$nROO + HO_2 \rightarrow nROOH + O_2$
38	$O_2 + iR \rightarrow OH + propoxide$
39	$CH_3OO + HO_2 \rightarrow CH_3OOH + O_2$

40	CH ₃ OOH → CH ₃ O + OH
41	$O_2QOOH_1 \rightarrow HO_2 + prod2$
42	CH ₃ CH ₂ OOH → ethoxy + OH
43	$H + RH \rightarrow H_2 + iR$
44	$QOOH_3 \rightarrow OH + propoxide$
45	$O_2 + iR \rightarrow QOOH_3$
46	ethoxy \rightarrow CH ₃ + CH ₂ O
47	$H + O_2(+M) \rightarrow HO_2(+M)$
48	$CH_3O + M \rightarrow CH_2O + H + M$
49	iRO → acetone + H
50	$O_2 + nR \rightarrow OH + propoxide$
51	$O_2 + QOOH_1 \rightarrow HO_2 + prod2$
52	$RH + CH_3O \rightarrow nR + CH_3OH$
53	nROO → OH + propoxide
54	$iROO + iROO \rightarrow O_2 + iRO + iRO$
55	$O_2QOOH_3 \rightarrow O_2 + QOOH_3$
56	$O_2 + QOOH_3 \rightarrow O_2QOOH_3$
57	$O_2QOOH_2 \rightarrow O_2 + QOOH_2$
58	$O_2 + QOOH_2 \Rightarrow O_2QOOH_2$
59	$O_2 + QOOH_1 \rightarrow O_2QOOH_1$
60	$O_2 + iR \rightarrow iROO$
61	$QOOH_1 \rightarrow nROO$
62	$nROO \rightarrow QOOH_1$
63	$O_2 + nR \rightarrow nROO$
64	vinoxylmethyl → allyloxy
65	allyloxy → vinoxylmethyl
66	$CH_2CH_2OH + O_2 \rightarrow O_2C_2H_4OH$
67	$O_2C_2H_4OH \rightarrow CH_2CH_2OH + O_2$
68	$acetylperoxy \rightarrow acetyl + O_2$
69	$acetyl + O_2 \rightarrow acetylperoxy$
70	$C_2H_5 + O_2 \rightarrow CH_3CH_2OO$
71	$CH_3 + O_2(+M) \rightarrow CH_3OO(+M)$
72	$CH_3OO + CH_2O \rightarrow CH_3OOH + HCO$
73	CH ₃ CH ₂ OO + CH ₂ O → CH ₃ CH ₂ OOH + HCO
74	iROO + CH ₂ O → iROOH + HCO

75	$nROO + CH_2O \rightarrow nROOH + HCO$
76	$HO_2 + C_3H_6 \rightarrow OH + propoxide$
77	$CH_3CH_2OO + HO_2 \rightarrow CH_3CH_2OOH + O_2$
78	$C_3H_6 + HO_2 \rightarrow propen1ol + OH$
79	$nROO + nROO \rightarrow O_2 + nRO + nRO$
80	$nROO + iROO \rightarrow O_2 + nRO + iRO$
81	CH ₃ OO + acetaldehyde → CH ₃ OOH+acetyl

IV. Convergence of Pathway Expansions

In Fig. 2 we show the time evolution of a number of species concentrations obtained from a conventional simulation where the initial conditions are P=10 bar, T=650K, and a stoichiometric mixture (φ=1) of C₃H₈ and air under adiabatic-isovolumetric conditions. These are similar conditions to those studied by Merchant et al [24]. The red curve shows the system temperature using the scale on the right of the figure. The two stage character of the ignition is clearly apparent with the first stage ignition exhibiting a temperature rise of about 100 K near 0.55 s followed by full ignition occurring at 0.77 s. Focusing on the carbon containing stable or metastable species depicted in the upper panel, the primary products during the early stages of the ignition process are propene (C₃H₆), formaldehyde (CH₂O), CO, acetaldehyde (CH₃CHO), and the ketohydroperoxide (OQ'OOH). We see that C₃H₆ is the main product near the beginning of the simulation, but CH₂O takes over as the largest carbon containing product at t=0.27 s, and eventually CO becomes the largest after t=0.65 s. The evolution of various carbon containing radicals is shown in the second panel. It is clear that the radical concentration growth shows two distinct exponential regimes during stage 1 (termed stages 1A and 1B by Merchant et al. [24]²⁴) and then sharply decreases during stage 2 before final ignition. The growth of the various HO_x species is depicted in the third panel that likewise exhibits two stage time-dependent ignition chemistry. It is found, as noted previously, that the chemistry underlying the ignition process qualitatively changes during the course of the reaction due to the temperature variation and the growth of secondary products. It is easily discovered, e.g., that the $HO_2+HO_2\rightarrow H_2O_2+O_2$ termination step greatly accelerates during the latter parts of stage 1 which effectively eliminates HO₂ as an attacking species of the propane fuel. Furthermore, the concentration of the OQ'OOH intermediate reaches a relative maximum near t=0.4 s and falls off quickly during stage 2, signaling a change in the efficiency of the cycle shown in Fig. 1. A factor in the negative temperature dependence occurring at the first ignition threshold is the shift in the quasi-equilibrium of the $R+O_2\leftrightarrow RO_2$ process toward the reagents which suppresses the growth of the radical pool. We are interested in using the evolution of the chemical pathways as an explanation for the changes in chemical behavior during the ignition process. As an overview, in Fig. 3 we show a

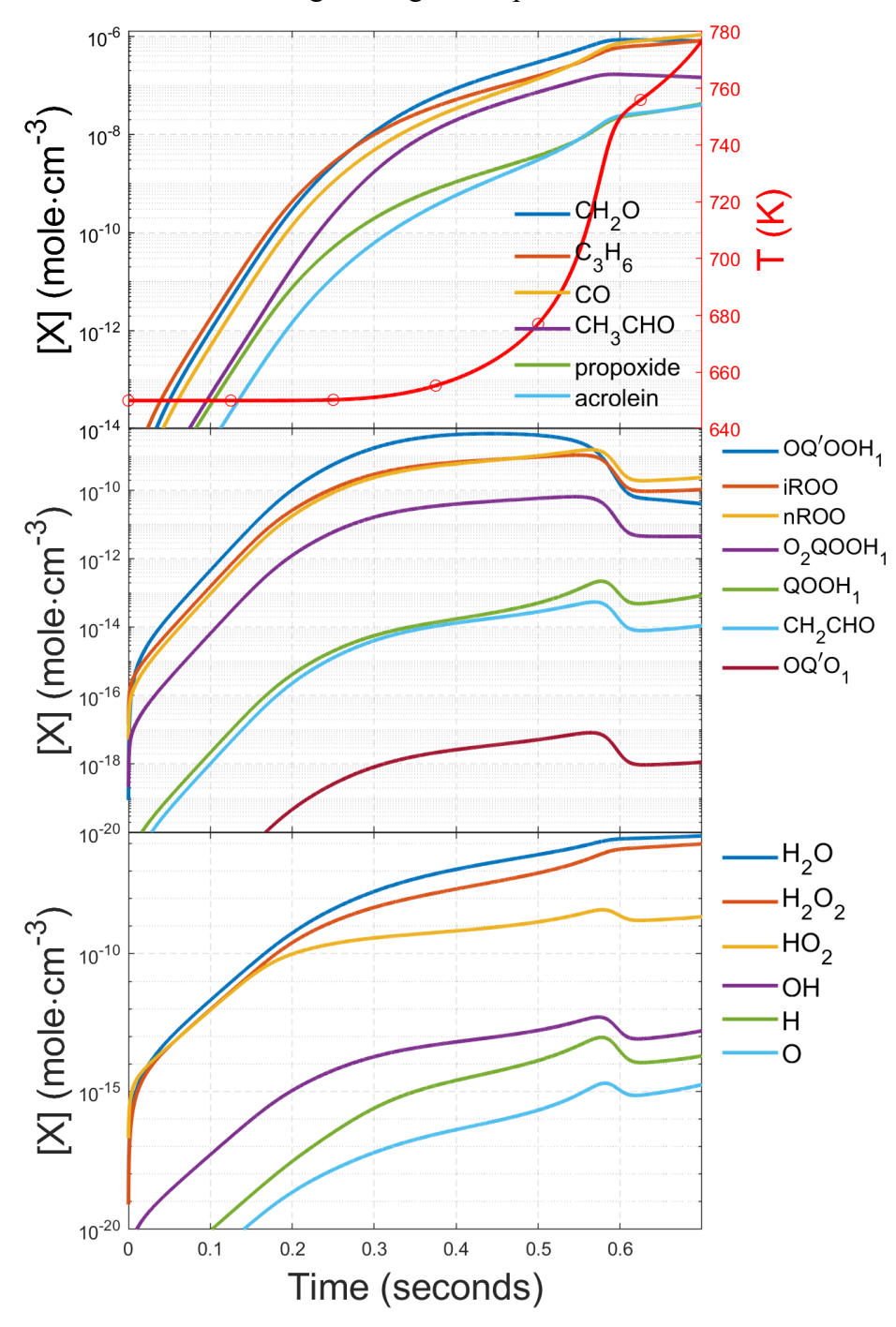
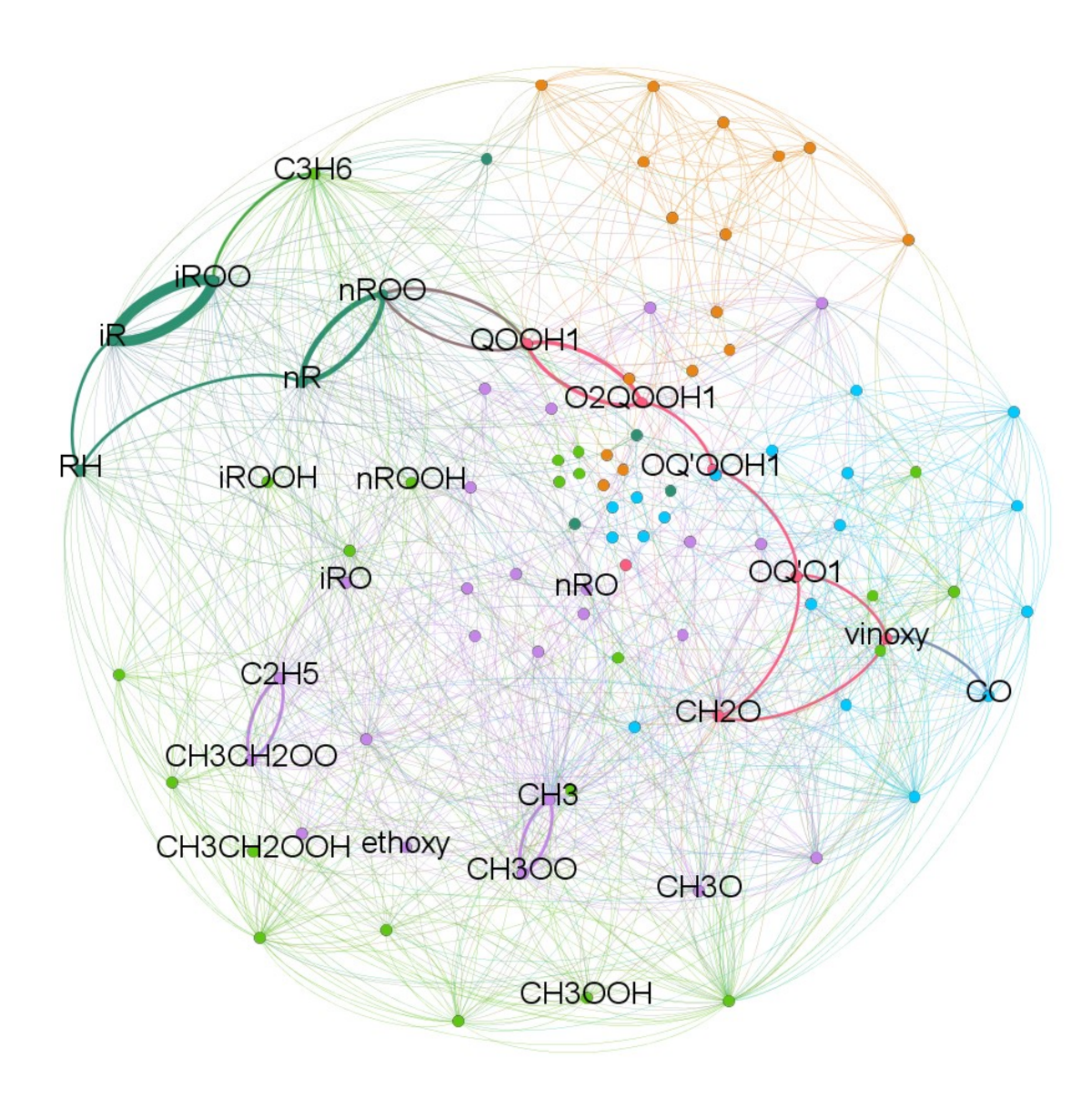
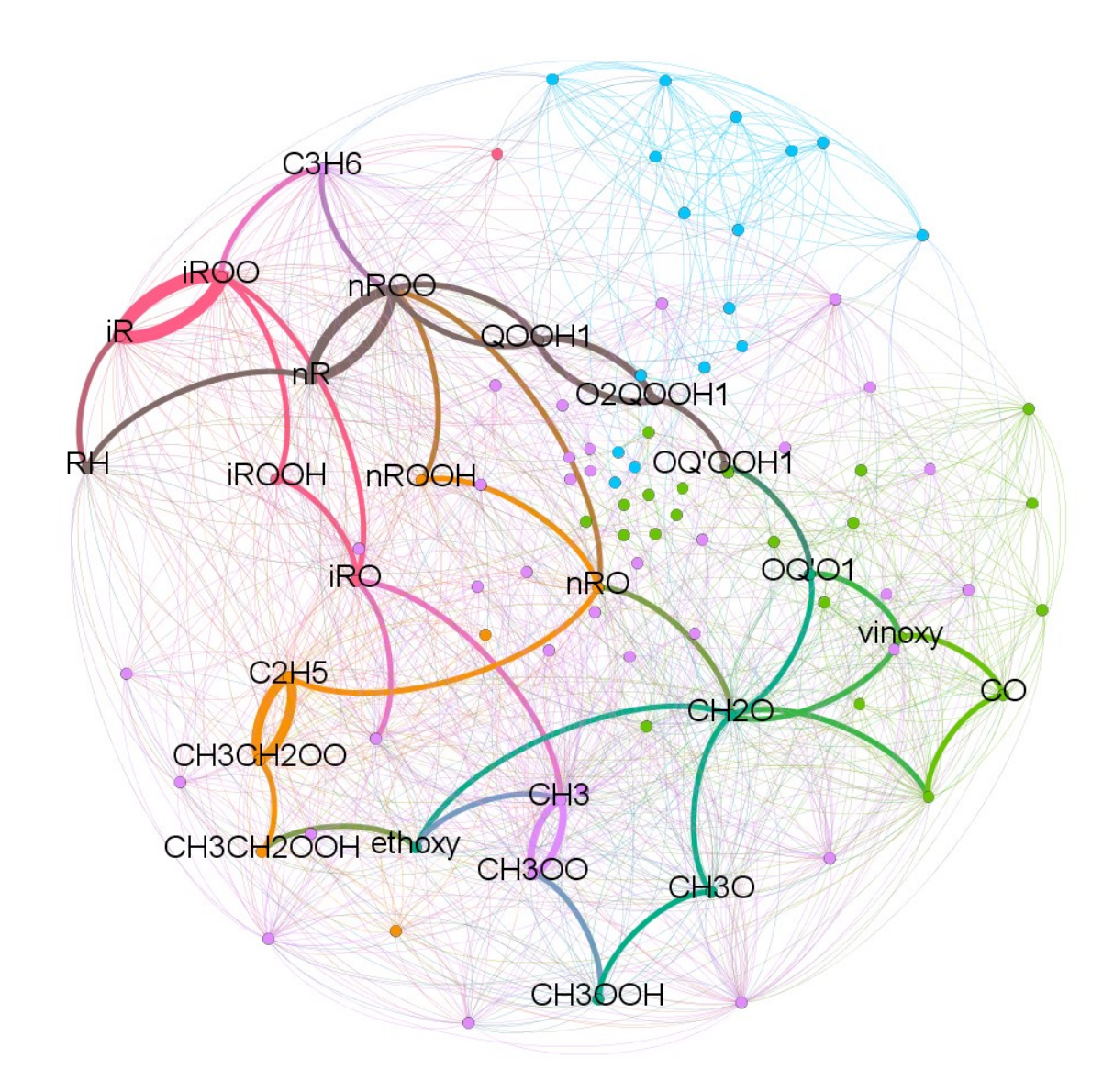
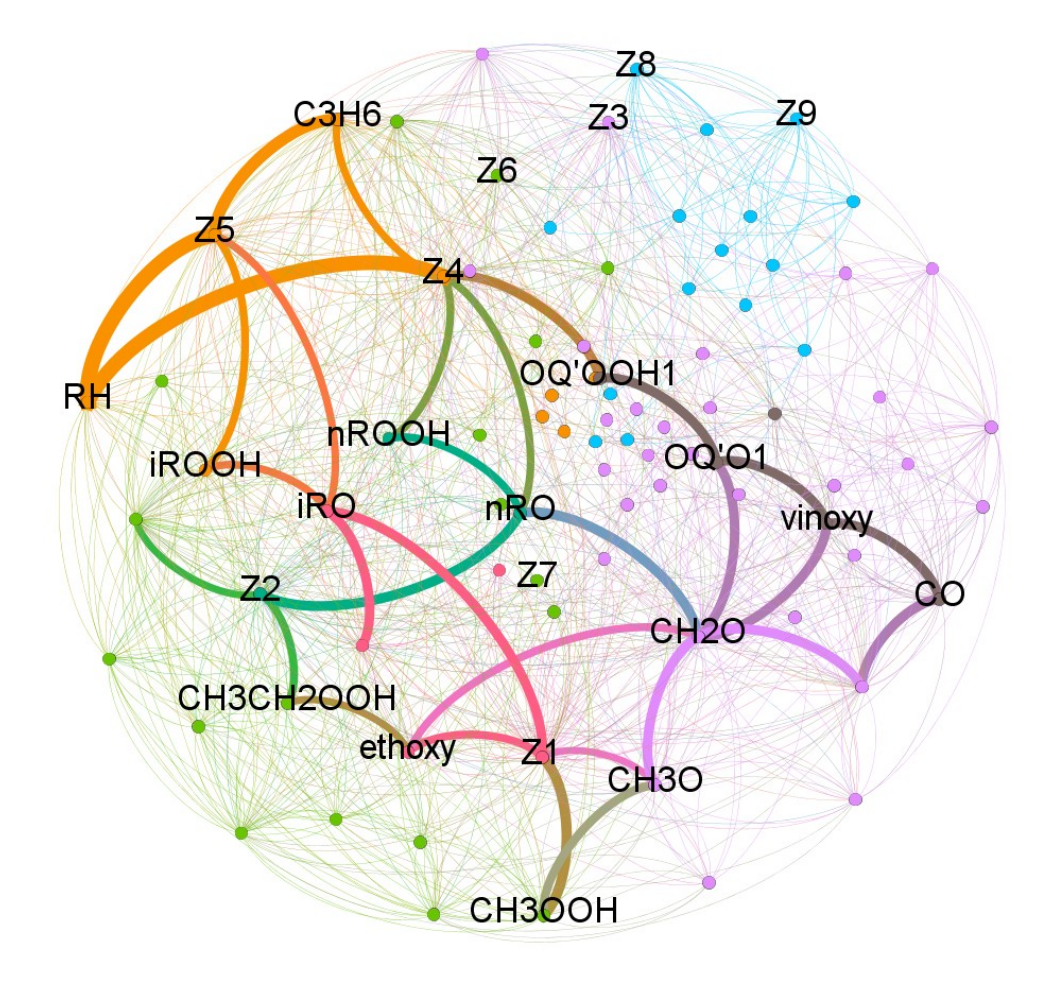


Fig. 2 Species concentrations versus time for propane ignition obtained at T=650K, p=10 bar, and ϕ =1 using a conventional kinetic simulation. The temperature is show as a red curve using the scale on the right hand side of the figure.





(b)



(c)

Fig. 3 The chemical graph for propane ignition. In (a) the graph is shown for stage one ignition (t=0.2s) and in (b) the graph is shown at a later time (t=0.5s). In panel (c) the t=0.5 graph is simplified using the CG's Z_1 - Z_9 . The adjacency in the graph is obtained by following a tagged carbon atom where the edges are elementary reaction steps, and the weights are obtained from the one-way rates using a stretched exponential scaling of the elementary steps. The thicker lines correspond to higher rates. Reactions with very small rates are omitted for clarity. The color coding and location of the nodes reflects the community structure of the graphs.

chemical graph created using the GEPHI software package [53] where adjacency on the graph is

defined by following chemically distinct carbon atoms. The carbon containing species are the vertices and the edges represent elementary reactions where the one-way instantaneous reaction rates are represented with line thickness with an exponential scaling factor. Figure 3a shows the graph evaluated at time t=0.2 s and Fig. 3b shows the graph at time t=0.5 s. The most *important* pathways delivering C-atoms to various species through this dynamical graph are apparent as connected sequences of the thick-edged reactions. In Fig. 3a, the primary catalytic cycle of the early stage ignition is clearly evident as C₃H₈ (designated as RH) moves sequentially through nR, nRO₂, QOOH₁, O₂QOOH₁, and OQ'OOH₁. The teardrop shaped edges connecting various adjacent vertices indicate important pairs of forward/reverse reactions. The coloring of the graph reflects the community structure revealed by the algorithm of Blondel et al. [54]. The flux moving off to the ineffective iR channel is also immediately seen as a second heavily weighted (dead end) branch coming from the C₃H₈ reagent in the upper left edge of Fig. 3a. In Fig. 3b, the graph is shown again at a later time (t=0.5 s) and clearly demonstrates an increase in the chemical complexity compared to Fig. 3a. The use of CG's (defined below in Table 2), in Fig. 3c, is seen to simplify the graph to some degree by contracting some of the most heavily weighted chattering pathways. The kinetics illustrated graphically in Fig. 3 demonstrate the growing level of chemical complexity through the increasing number of important competing chemical pathways. The challenge is then to extract and quantify these pathways.

Table 2. Chattering groups for the propane mechanism. The indices of the component species and the primary formation/decay reaction are indicated.

	Species Name	Reaction Index	Primary Reactions
Group 1			
	CH ₃	71	$CH_3 + O_2(+M) \rightarrow CH_3OO(+M)$
	CH ₃ OO	30	$CH_3OO(+M) \rightarrow CH_3 + O_2(+M)$
Group 2			
	C ₂ H ₅	70	$C_2H_5 + O_2 \rightarrow CH_3CH_2OO$
	CH ₃ CH ₂ OO	31	$CH_3CH_2OO \rightarrow C_2H_5 + O_2$
Group 3			

	Acetyl	69	$acetyl + O_2 \rightarrow acetylperoxy$
	Acetylperoxy	68	acetylperoxy → acetyl + O ₂
Group 4			
	nR	63	$O_2 + nR \rightarrow nROO$
	nROO	10	$nROO \rightarrow O_2 + nR$
		62	nROO → QOOH ₁
		61	QOOH₁ → nROO
	$QOOH_1$	59	$O_2 + QOOH_1 \rightarrow O_2QOOH_1$
	O_2QOOH_1	7	$O_2QOOH_1 \rightarrow O_2 + QOOH_1$
Group 5			
	iR	60	$O_2 + iR \rightarrow iROO$
	iROO	6	$iROO \rightarrow O_2 + iR$
Group 6			
	Allyloxy	65	allyloxy → vinoxylmethyl
	Vinoxylmethyl	64	vinoxylmethyl → allyloxy
Group 7			
	O ₂ C ₂ H ₄ OH	67	$O_2C_2H_4OH \rightarrow CH_2CH_2OH + O_2$
	CH ₂ CH ₂ OH	66	$CH_2CH_2OH + O_2 \rightarrow O_2C_2H_4OH$
Group 8			
	QOOH ₂	58	$O_2 + QOOH_2 \rightarrow O_2QOOH_2$
	O ₂ QOOH ₂	57	$O_2QOOH_2 \rightarrow O_2 + QOOH_2$
Group 9			
	QOOH ₃	56	$O_2 + QOOH_3 \rightarrow O_2QOOH_3$
	O ₂ QOOH ₃	55	$O_2QOOH_3 \rightarrow O_2 + QOOH_3$

Figure 4 show another manifestation of the evolving dynamical character of the kinetics, the change in lifetimes of a number of intermediates, defined as the inverse instantaneous decay rate. These instantaneous lifetimes reflect the sum of rates for all the sink reactions that deplete those species, i.e.

$$\tau_{i}(t) = \frac{1}{k_{i}(t)} = \frac{1}{\sum_{l}^{sink} \omega_{l}^{i}(t) / [X_{i}(t)]}$$
(10)

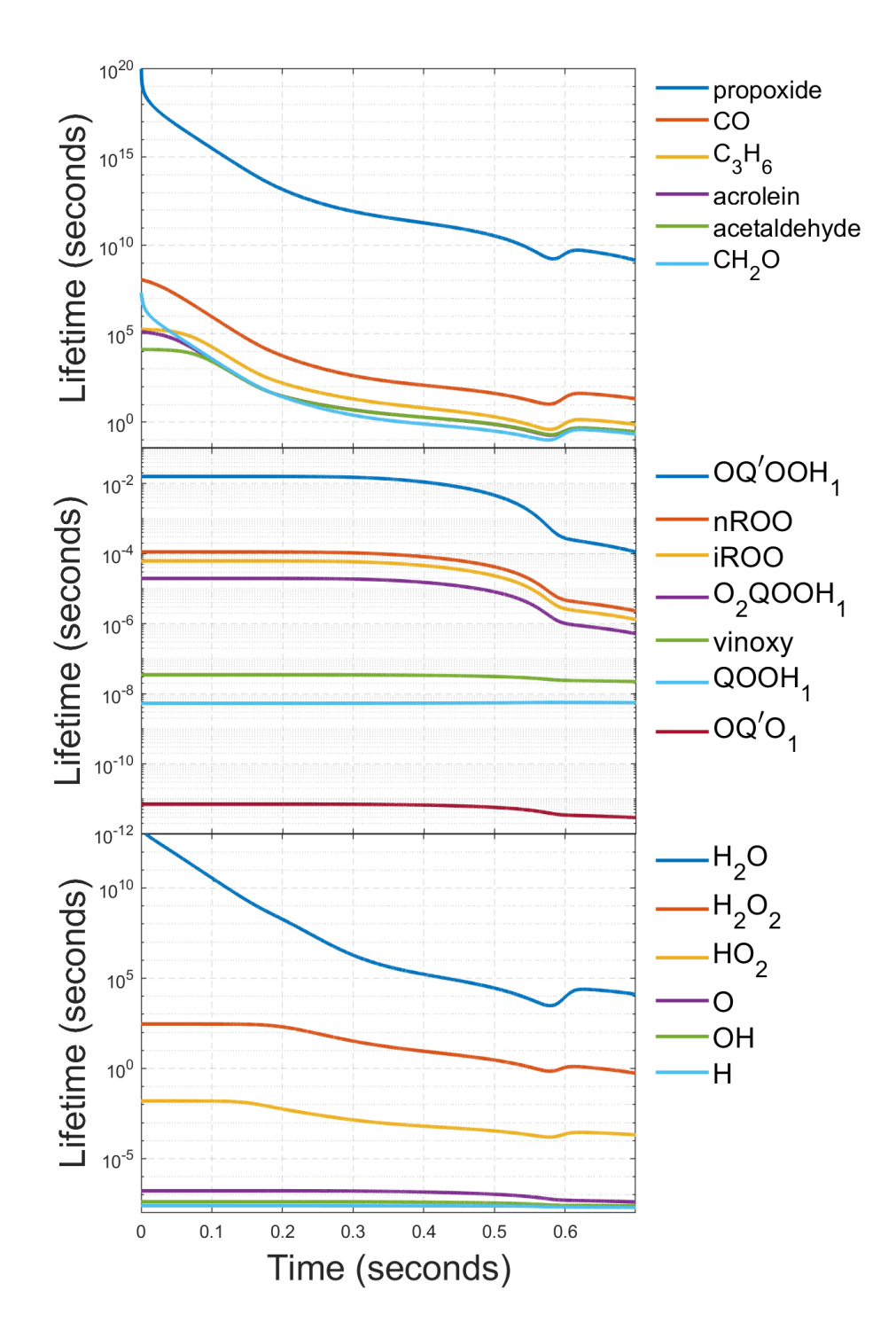


Fig. 4 The species lifetime $1/k_{decay}(t)$ as a function of time for a variety of chemical species for propane/air ignition at T=650 K, P=10 bar, and Φ =1. It is clearly seen that many species exhibit variations of orders of magnitude in species lifetime during different phases of the ignition process.

The plot clearly reveals a strong temporal evolution of the decay rates. The species non-reaction probability $\mathcal{P}_i(t_a, t_b)$ is the exponential function of the time-integral of the decay rate, $-\int_{t_a}^{t_b} k_i(t)dt$, which is a key quantity in SOHR. As we shall see, the time-dependent character [55, 56, 57] of the graph can significantly alter the overall reaction mechanism. The trends in species lifetimes shown in Fig. 4 reflect the kinetic stabilities with the stable species surviving for timescales that are several orders of magnitudes larger than the free radicals. The anomalously large lifetime for the propoxide is due to the absence of effective consumption reactions for this species in the kinetics model [24].

A large number of carbon following chemical pathways connecting the propane reagent to the possible products and intermediates were numerically generated along with their probabilities using the MC methods outlined above. The pathways obtained were assessed and grouped using a simple symbolic representation. The CG's were quickly identified from the pathways that exhibited recurring sequences of steps. All subsequent primitive and merged pathway results were then automatically contracted. As described above, a pathway passing through any member of the CG was automatically combined with all possible chattering paths involving "interior reactions" of the CG to yield a single path and a fully summed probability. The nine CG's found are listed in Table 2 which are cross-referenced with the reaction and species indices of the propane mechanism. [Forward and backward reactions are listed separately for several important reactions but are related by microreversibility.] Many of these CG's involve simply a pair of combination/dissociation reactions of a radical with O₂, e.g. CH₃+O₂↔CH₃OO. One CG, however, involves the interconversion of four species: nR, nRO₂, QOOH₁, and O₂QOOH₁, which is shown in Fig. 5. This is an important CG since it comprises a large portion of the primary catalytic cycle shown in Fig. 1. An essential concept is that the CG is a single entity that is treated as one chemical species in much the same way that individual quantum states are internal parts of a single molecule. Any entering or exiting flux into or out of the CG quickly equilibrates losing memory of the particular entering or exiting species.

The SOHR methodology brings out the dynamical characteristics of the kinetics by quantifying the mechanistic chemical paths as functions of time. The pathway probabilities for ten of the highest probability reaction routes are plotted in Fig. 6. These routes are listed in Table 3.

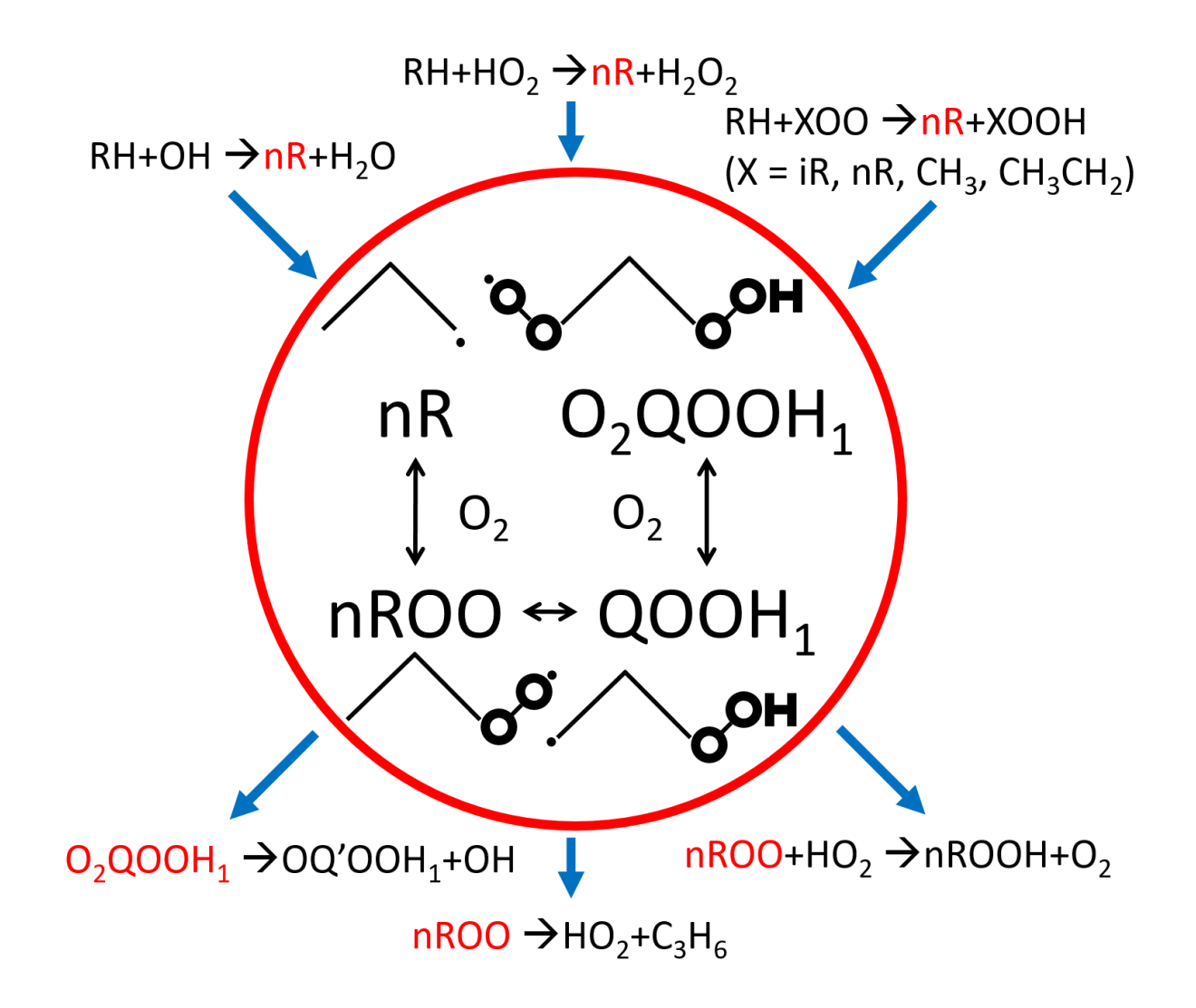


Fig. 5 The \underline{CG} Z_4 = (nR, nROO, QOOH₁, O₂QOOH₁). The kinetics of these four species behave as a single entity with main production sources being formation of nR radicals by OH+RH and HO₂+RH. The main sinks of Z_4 are O₂QOOH₁ \rightarrow OH+OQ'OOH₁, nROO \rightarrow HO₂+propene, and nROO+HO₂ \rightarrow nROOH+O₂.

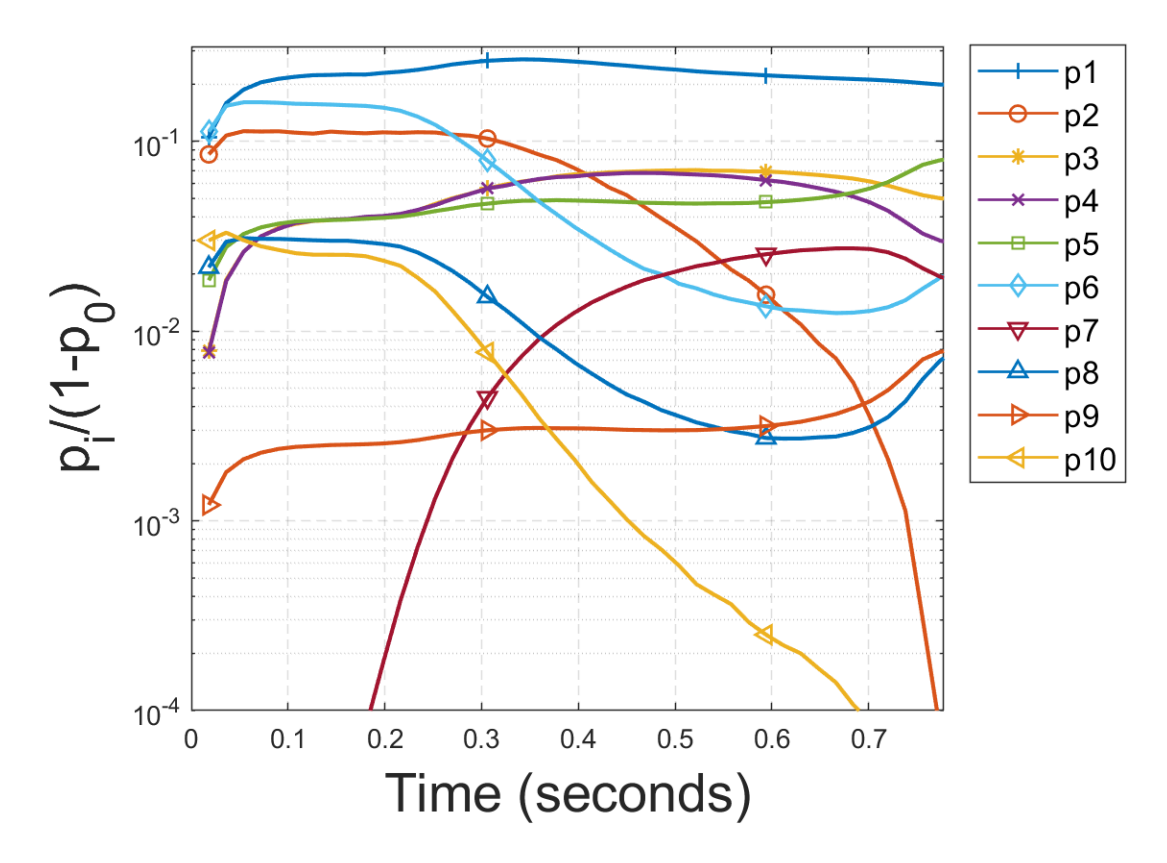


Fig. 6 Pathway probabilities as a function of time for ten of the most important carbon-atom following chemical paths, p1-p10. The pathways are listed in Table 3 and the reaction indices are given in Table 1. (Several high probability pathways are omitted since they are virtually identical to one of the paths p1-p10).

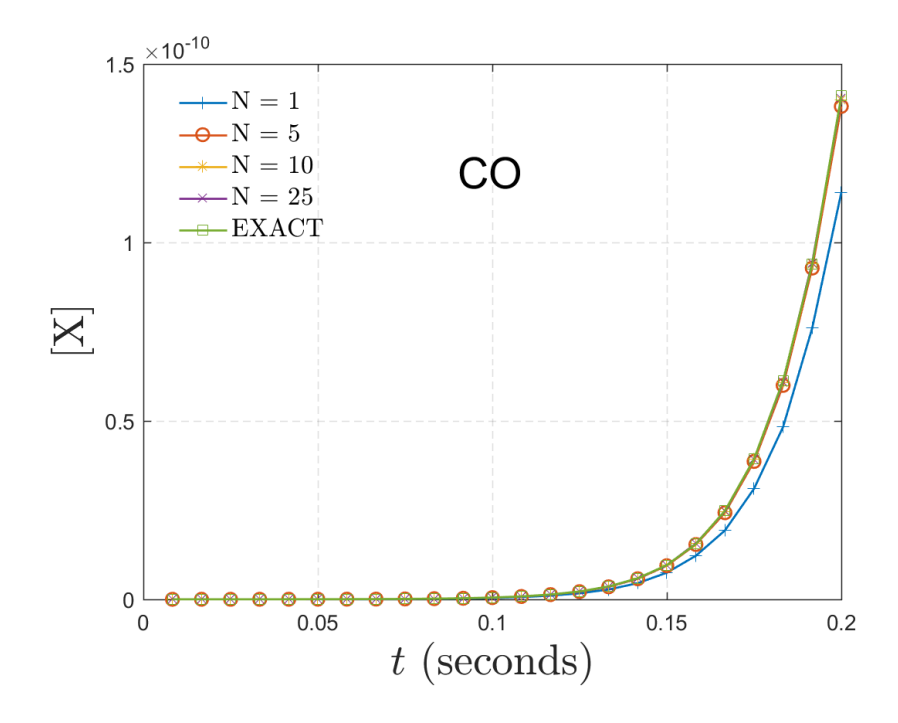
Table 3. Ten important carbon following pathways that originate with propane and terminate in a stable or metastable species. The CG's are given in Table 2, and the designation $Z_n(S_i,S_j)$ indicates the n^{th} CG where S_i is the entering species S_j is the exiting species.

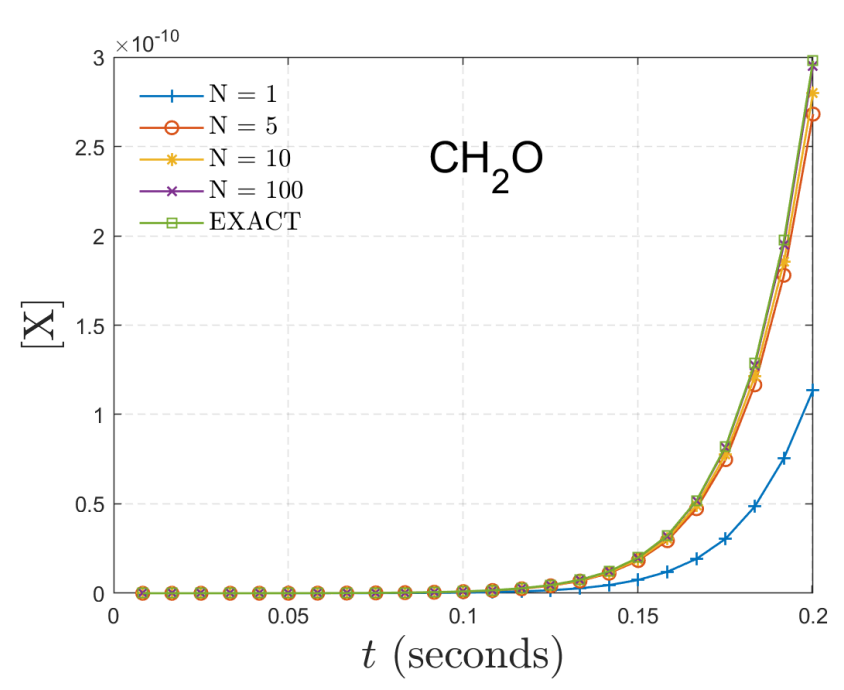
1	$RH \xrightarrow{R4} Z_5(iR, iROO) \xrightarrow{R16} C_3H_6$
2	$RH \xrightarrow{R3} Z_4(nR, O_2QOOH_1) \xrightarrow{R11} OQ'OOH_1$
3	$RH \xrightarrow{R3} Z_4(nR, O_2QOOH_1) \xrightarrow{R11} OQ'OOH_1 \xrightarrow{R18} OQ'O_1 \xrightarrow{R22} vinoxy \xrightarrow{R27} CO$
4	$RH \xrightarrow{R3} Z_4(nR, O_2QOOH_1) \xrightarrow{R11} OQ'OOH_1 \xrightarrow{R18} OQ'O_1 \xrightarrow{R22} CH_2O$
5	$RH \xrightarrow{R3} Z_4(nR, nROO) \xrightarrow{R32} C_3H_6$

6	$RH \xrightarrow{R5} Z_5(iR, iROO) \xrightarrow{R16} C_3H_6$
7	$RH \xrightarrow{R4} Z_5(iR, iROO) \xrightarrow{R35} iROOH \xrightarrow{R17} iRO \xrightarrow{R23} acetaldehyde$
8	$RH \xrightarrow{R5} Z_5(iR, iR) \xrightarrow{R9} C_3H_6$
9	$RH \xrightarrow{R3} Z_4(nR, nR) \xrightarrow{R28} C_3H_6$
10	$RH \xrightarrow{R8} Z_4(nR, O_2QOOH_1) \xrightarrow{R11} OQ'OOH_1$

The CG are denoted by $Z_n(S_i,S_i)$, where the index n given in Table 2. Transitions inside the CG are not included in the path since they are summed out. The species S_i in this notation is the entering species and S_i is the exiting species into, and out of, the CG. The pathways follow carbon atoms from propane (defined as time t=0) to other species at a later time t and all found to terminate in long-lived intermediates. The probabilities are normalized using $1-P_0$ where P_0 is the non-reaction probability of propane at time t. It is seen that the preferred reaction paths depend very strongly on time and the probabilities show numerous crossings. At very early times, paths p1 and p6 are nearly equal in probability, reflecting roughtly equal branching into the nR and iR isomers. The path p1 terminates in the metastable species OQ'OOH₁ while p6 goes to propene following fission of iRO₂. The iR following path p1 quickly begins to outstrip the other paths as the p6 probability declines when OQ'OOH1 starts to fragment and distributes the carbon atoms to other species. We should note that the highest probability carbon-following pathways shown here, all of which go to long-lived intermediates, would not be the pathways used to describe production of transient intermediates (like CHO) that follow other routes. If the 50 most important pathways (terminating in any carbon-containing species) are computed, it is found that well over 95% of the total probability flux is already obtained.

We have established that a manageable number of paths can satisfactorily quantitatively account for the observed concentrations that occur during the ignition phase. In Fig. 7 we show the convergence of the concentration versus time for the long-lifetime stable species CO, CH₂O, and C₃H₆. It is seen that the concentrations converge uniformly during the early times (t<0.2 s) with relatively few pathways, usually fewer than 10 to achieve accuracy of a few percent. At longer times more pathways become required as various more indirect routes begin to contribute. Several hundred pathways may be required for similar accuracy at late stage ignition. The use of merged pathways in which similar reaction steps are lumped together can greatly reduce the number of





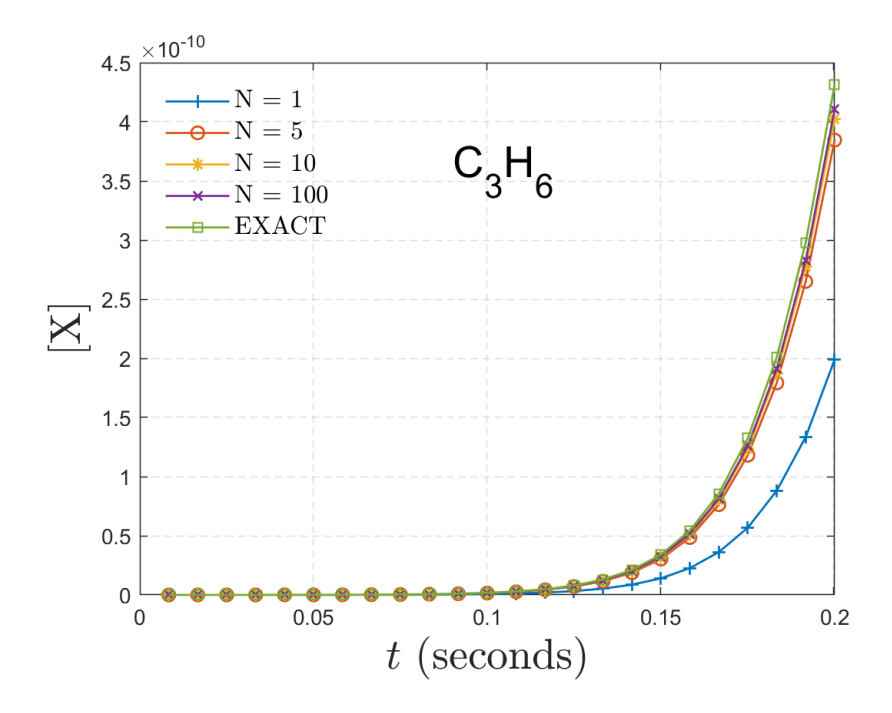


Fig. 7 The concentration of the CO, CH₂O, and C₃H₆ closed shell product species versus time obtained by SOHR as a function of the number of primitive carbon following pathways that initiate with C₃H₈ and terminate with CO. The SOHR method is seen to converge rapidly to the exact result, obtained by conventional kinetic simulation, during stage 1 of ignition.

required pathways, often by factors of 10. The convergence at later times is illustrated in the Supporting Information.

V. The Quasi-steady-state Model of Chattering Groups

The contraction of rapidly interconverting chattering pathways is required for the efficient performance of the SOHR for the present problem. The combining of chattering paths is not an approximation *per se*, but is rather a reordering of the infinite summation over pathways used in computing the observables via eq. (7). Thus if the exact reference trajectory is used to compute the net probability of the merged pathway, it would yield the same as that obtained from the infinite sum over chattering paths. Nevertheless, the CG concept and the choice of constituent species is closely related to the notion of the quasi-steady-state approximation (QSSA). To emphasize this, consider the key CG Z₄ consisting of nR, nRO₂, QOOH₁, and O₂QOOH₁ which we identified from the pathway simulation. The interconversion rates between these species are much higher than the

net decay rate from the group. In Fig. 8 we show the instantaneous species lifetime for these four constituents along with net lifetime of the merged CG. Interestingly, the net lifetime of this key group Z_4 stays constant (dominately via the reaction $O_2QOOH_1 \rightarrow OH+OQ'OOH$) until 0.2 s beyond which there is a noticeable growth in the decay rate. Merchant et al. [24] hypothesize that at t > 0.2 s, HO_2 recombination becomes the dominant HO_2 consumption channel, and this then represents the transition from stage-1A to stage-1B. Alternately, the present lifetime analysis indicates that the transition from stage-1A to stage-1B may instead be driven by new decay channels of Z_4 .

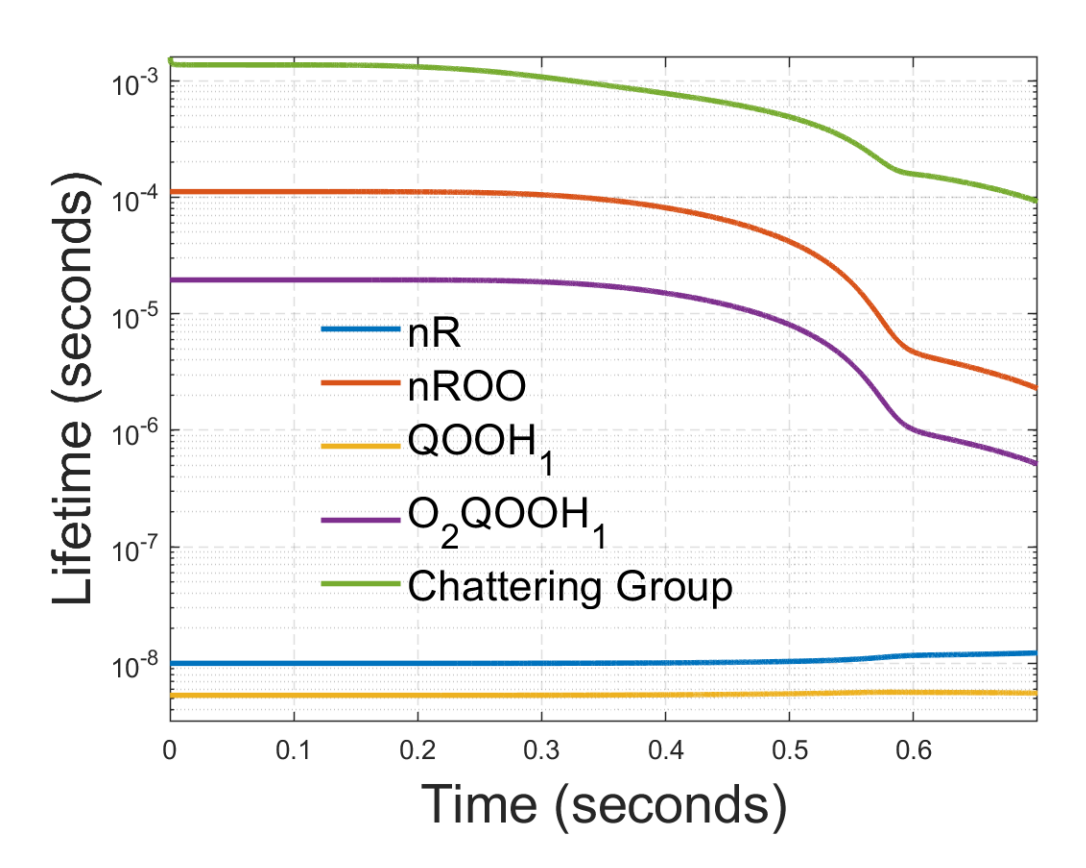


Fig. 8. Species lifetime for the group Z_4 and its constituent species, nR, nRO_2 , $QOOH_1$, O_2QOOH_1 . It is seen that the overall lifetime Z_4 is a factor of 20 longer than the next longest lived species, nRO_2 .

We see the group as a whole is more than one order of magnitude more stable than any of the individual species. At early times, t < 0.3 s, the overall lifetime of the CG is roughly 2×10^{-3} s,

while the most stable constituent species nRO_2 has a lifetime of $1\times10^{-4}s$. Hence we expect that a quasisteady state concentration profile will develop within the group regardless of whether the CG is in steady state with the other components of the system. As a test of this approximation, Fig. 9 shows the relative concentration of these four species along with the QSSA. The QSSA approximation used here is the simplest four species steady state model, i.e. where the rate equations of the four concentrations nR, nRO_2 , $QOOH_1$, and O_2QOOH_1 are set to zero and the equations are solved numerically. The QSSA used here is decoupled from other radical species not lying in the same CG. The relative concentration of the four species are locked together as the flux quickly shuttles between the members for the CG. While the relative concentrations are quite stable, it bears remembering that the individual radical concentrations are growing exponentially with time. The relative concentrations with the CG remains synchronized through the first ignition threshold and is useful up to the point of full ignition. Also shown in Fig. 9 are dashed lines labeled as K_{eq} that indicate the concentrations predicted by a pairwise local equilibrations between $nR+O_2 \leftrightarrow nRO_2$, $nRO_2 \leftrightarrow QOOH_1$, and $O_2+QOOH_1 \leftrightarrow O_2QOOH_1$. It is seen that the CG taken as a set of four species is a much more accurate representation of the kinetics than the pairwise analysis.

VI. Catalytic Cycles for the OH-Radical

A. Overview

The production and destruction of OH is centrally important for the growth of the radical pool responsible for autoignition. During stage 1 of the ignition process, the breakdown of C₃H₈ is most commonly initiated by an attack by either OH or HO₂ radicals to yield a propyl radical. At T=650 K and P= 10 bar, OH is roughly 10⁵ times more reactive than HO₂, but has a concentration 10⁵ smaller than HO₂ precisely because HO₂ is less reactive and accumulates. Hence, the production of a "new" OH radical is much more effective in promoting ignition than the production of a new HO₂ radical and it makes sense to focus on the auto-catalytic cycle where OH is the carrier. The largest source and sink reactions for OH are plotted as fractions of the total rates versus time in Figs. 10 and 11, respectively. As seen in Fig. 11, during stage 1 of the ignition, OH is primarily consumed by reaction with propane yielding the i-propyl (iR) and n-propyl (nR) radical isomers in roughly equal amounts. At later times, OH begins to react with secondary products, mostly the metastable species CH₂O, C₃H₆, H₂O₂, and HO₂ although the reaction rate with propane

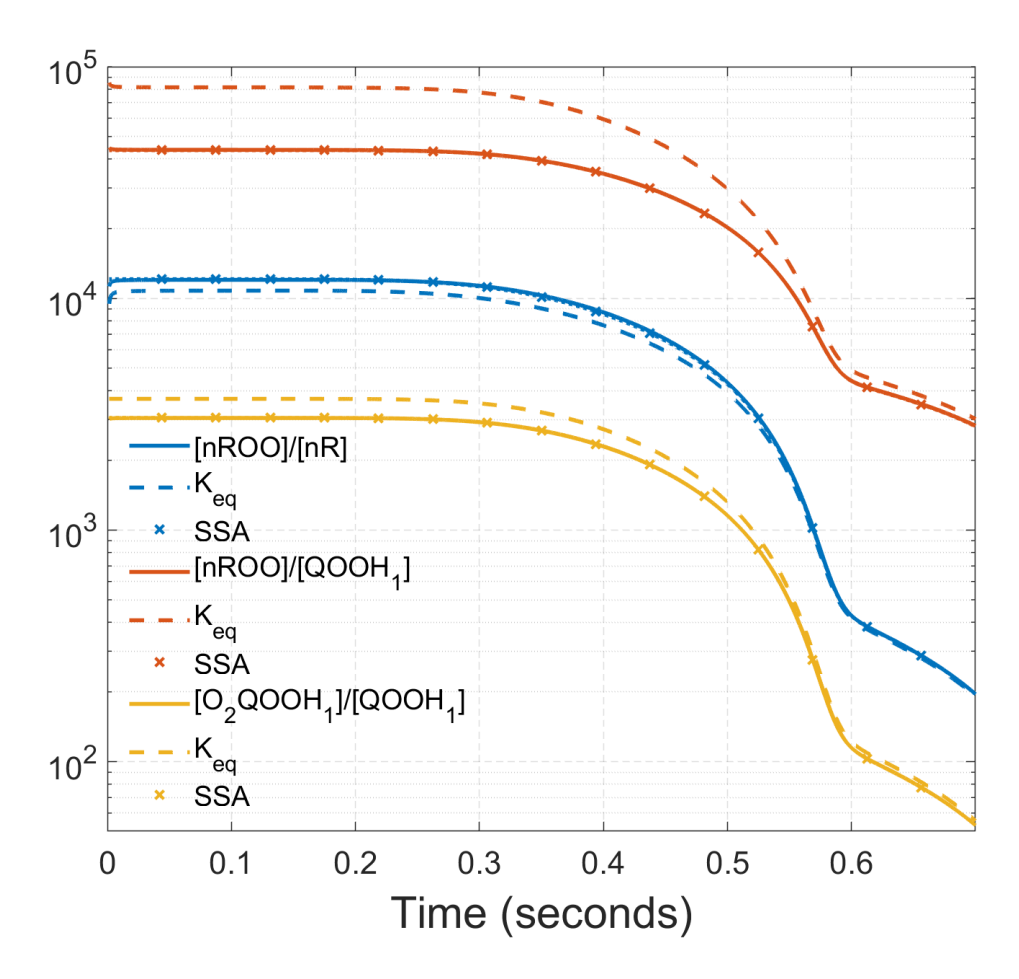


Fig. 9. The concentration ratio of species within the CG Z_4 as a function of time. The exact concentration ratios are shown with solid lines, the quasi-steady state approximation is shown with symbols, and the prediction of the equilibrium approximation is shown with dashed lines.

remains the largest until the ignition threshold. The primary sources of OH, shown in Fig. 10, are quite different during the first and second ignition stages. The early time OH production is dominated by the three processes $O_2QOOH_1 \rightarrow OH + OQ'OOH_1$, $OQ'OOH_1 \rightarrow OH + OQ'O$, and $CH_2CHO+O_2 \rightarrow OH + CO+CH_2O$. These are the first, second, and third OH-producing reactions of the primary cycle depicted in Fig. 1. The first process is the most efficient, as might be expected, since the second and third steps of the cycle are contingent on the first. Also contributing at early times are the decomposition reactions of the propyl hydroperoxy species, nC_3H_7OOH and iC_3H_7OOH . During the second stage of ignition, the decomposition of the methyl hydroperoxy

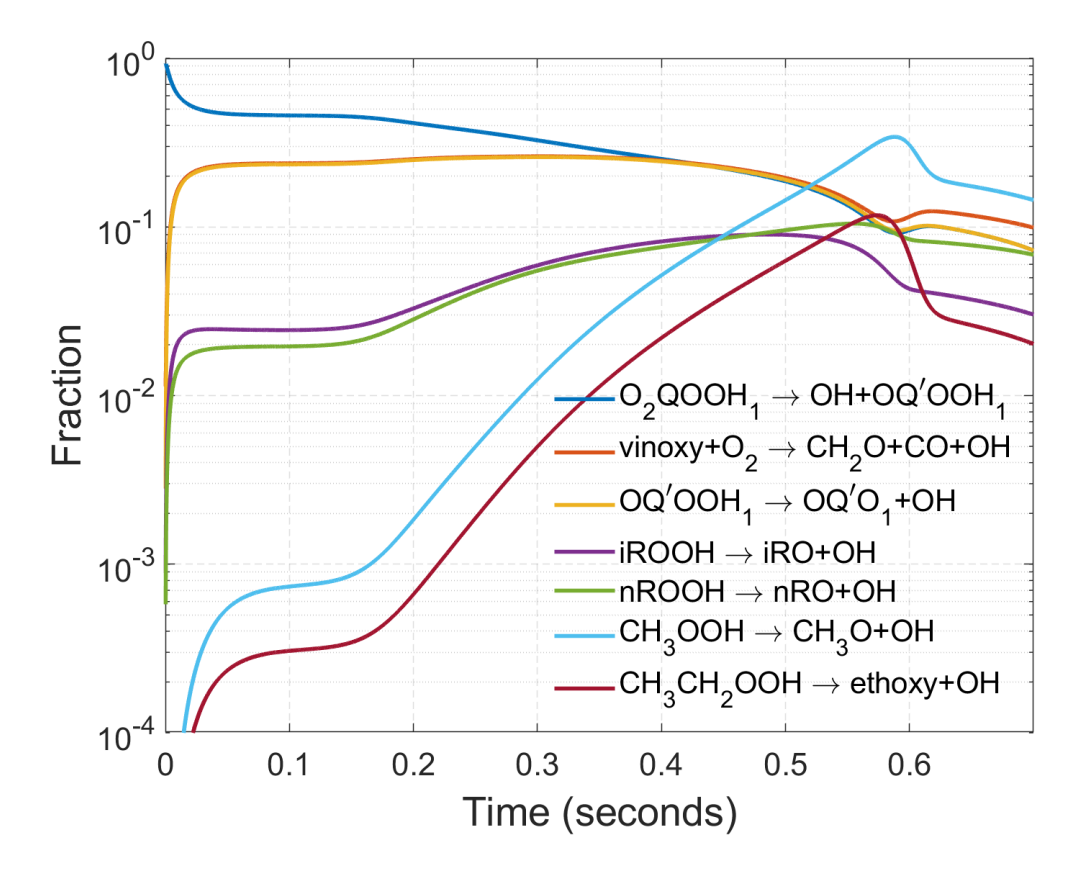


Fig. 10. Source reactions producing OH expressed as fractions of the total. The fraction indicates the ratio $\omega_i(t)/\sum_j \omega_j(t)$ where $\omega_i(t)$ are the rates of the source reactions for OH and sum is over all sources.

species becomes the largest single source of OH, i.e. $CH_3OOH \rightarrow CH_3O+OH$. Also contributing significantly during the second stage of ignition is the decomposition of ethyl hydroperoxide, $C_2H_5OOH \rightarrow C_2H_5O+OH$, and other hydroperoxides such as H_2O_2 . These "secondary" OH sources suggest that a different mechanistic interpretation than the standard picture (i.e. Fig. 1) is required to understand low temperature ignition at these later times.

During early (stage 1A) times, we confirm that the low-temperature ignition chemistry behind the OH production largely follows the scenario outlined by Merchant *et al.*[24]. The nascent propyl radicals nR and iR quickly associate with O₂ to form the peroxy radicals nRO₂ and iRO₂. The nRO₂ radical, which is part of the Z₄ group, can produce up to three highly reactive OH radicals by the cycles sketched in Fig. 1. The iRO₂ radical, on the other hand, reacts

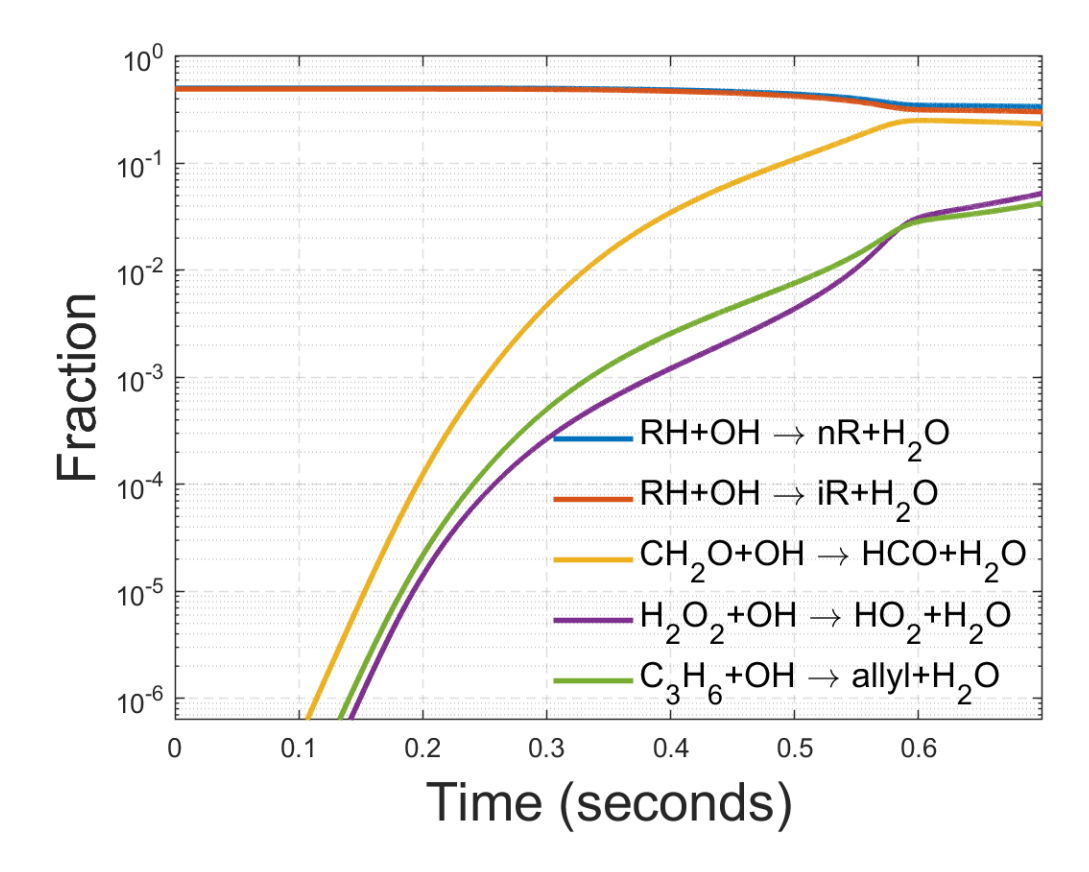


Fig. 11. Sink reactions consuming OH expressed as fractions of the total. The fraction indicates the ratio $\omega_i(t)/\sum_j \omega_j(t)$ where $\omega_i(t)$ are the rates of the sink reactions for OH and sum is over all sinks.

more slowly and produces less reactive byproducts such as HO₂. The newly generated OH and (to a lesser extent) HO₂ radicals can then attack C₃H₈ molecules and renew the cycle. The efficiency of this catalytic cycle affects the rate of exponential growth of the radical pool and plays a determining role in the occurrence of the second ignition phase.

We can assess the efficiency and completeness of the OH-catalytic cycle using the pathway perspective provided by the SOHR method. This approach is attractive since the precise multistep mechanism of OH-generation is then directly inferred from the chemical pathways. In particular, we can distinguish between OH production from pathways within the primary catalytic cycle depicted in Fig. 1 and other more circuitous routes in the kinetics. The OH production rate corresponding to the particular pathway that terminates with the OH species as a co-product (along

with a carbon containing species S_n) in the final reaction step, R_n , is obtained as discussed in Sec. IIC. The cumulative probability $\chi_j(t,t+\delta)$ is the total probability of arriving at species S_n (and hence producing an OH-radical) via pathway j at any time between t and $t+\delta$ starting from the initial species of the cycle (typically nR or iR) at time t. We expect that $\chi_j(t,t+\delta)$ will become quickly independent of δ once δ is longer than all the chemical lifetimes of species along the pathways. On the other hand, when the chemistry involves long-lived secondary species, a significant time lag may occur between the initiation reaction and the arrival at the terminal species. Then, the steady state picture of catalytic chain branching becomes suspect. The relevant timescale for the present problem is set by the ignition delay time of 0.77 s. In order to gauge the importance of various pathways a value of δt must be set. A modest value of δt =0.1s was selected to screen the importance of various pathways. The catalytic efficiency γ (discussed in Sec. IIC) is also dependent on the contingent probability of the OH-radical regenerating the cycle, denoted by $\alpha(t)$. For the primary cycle $\alpha(t)$ represents the branching ratio that the OH-radical produces an nR radical upon reaction with any species in the mixture. A cycle originating with the iR radical would define $\alpha(t)$ to be the branching ratio for the OH reaction to form iR radical.

Figure 12 shows $\alpha(t) \cdot \chi_j(t, t + \delta = 0.1)$, i.e. the contribution to $\gamma(t)$ from path j, computed for the 10 most important pathways. The pathways in Fig. 12 are constrained to yield an OH-radical as a co-product of the final step, while those shown previously in Fig. 6 were permitted to go to *any* possible carbon containing product. The pathways used in Fig. 12 are listed in Table 4. These reaction routes identify the most important sources of OH. Each of the pathways begins with the formation of either an nR-radical (paths mP₁-mP₅) or an iR-radical (paths mP₆-mP₁₀) and then follow distinct chemical routes to OH-production. In these pathways the nR reactions dominate at early times and the iR reactions become appreciable at later times.

It is straightforward to construct a more complete diagram for the OH producing catalytic cycles than the primary route of Fig. 1 using the pathways obtained in Fig. 12. In Fig. 13, we arrange the pathways making explicit use of the CG's Z₁=(CH₃,CH₃OO), Z₂=(CH₃CH₂, CH₃CH₂OO), Z₄=(nR, nROO, QOOH₁, O₂QOOH₁), and Z₅=(iR, iROO). The individual reactions connecting the various species are shown in small circles using the reaction labels from Table 1. The pathways, that include both species and reaction labels, are given in Table 4. It is seen that the three most important paths (mP1, mP2, mP3) from Fig. 12 comprise the

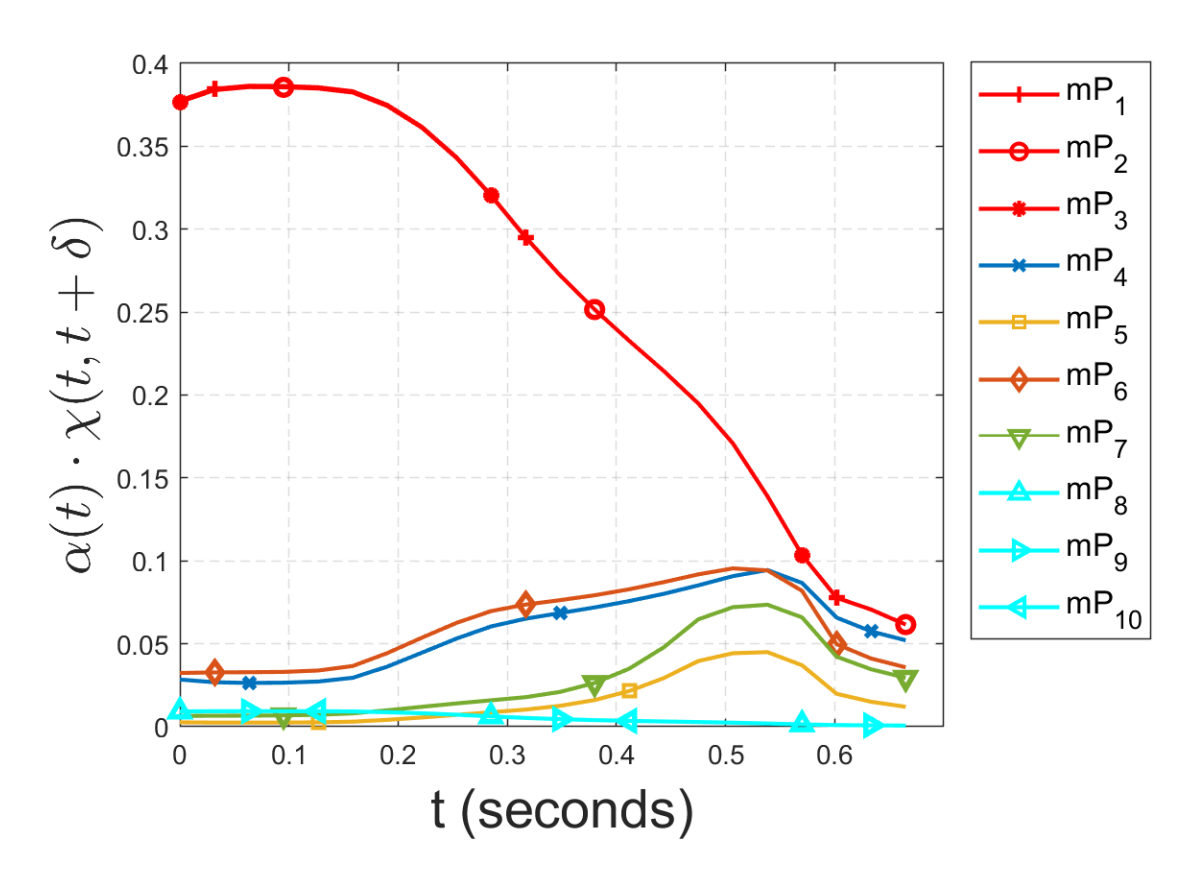


Fig. 12. The contributions to the catalylic efficiency, $\gamma = \alpha \cdot \chi - 1$, from the 10 most important merged chemical pathways listed in Table 4. The pathways mP₁, mP₂, and mP₃ are seen to be very close in value.

Table 4. Most important chemical pathways at T=650 K and p=10 bar originating with propane (RH) that generate OH as a co-product in the final step. The pathways are merged over all reactions that connect a given reagent to a given product. These pathways are shown graphically in Fig. 13 and constitute the main catalytic cycles.

Path	Primary Cycle
1	OH +RH $\stackrel{R3}{\rightarrow}$ Z ₄ (nR, O ₂ QOOH ₁) $\stackrel{R11}{\longrightarrow}$ OQ'OOH ₁ + OH
2	OH +RH $\stackrel{R3}{\rightarrow}$ Z ₄ (nR, O ₂ QOOH ₁) $\stackrel{R11}{\longrightarrow}$ OQ'OOH ₁ $\stackrel{R18}{\longrightarrow}$ OQ'O ₁ + OH
3	OH +RH $\stackrel{R3}{\rightarrow}$ Z ₄ (nR, O ₂ QOOH ₁) $\stackrel{R11}{\longrightarrow}$ OQ'OOH ₁ $\stackrel{R18}{\longrightarrow}$ OQ'O ₁ $\stackrel{R22}{\longrightarrow}$ vinoxy $\stackrel{R27}{\longrightarrow}$ CO+ OH
	Spur Cycle 1
4	OH +RH $\stackrel{R3}{\rightarrow}$ Z ₄ (nR, nROO) $\stackrel{R12,R21,R37,R75}{\longrightarrow}$ nROOH $\stackrel{R20}{\longrightarrow}$ nROO+ OH

	Spur Cycle 2
5	$\begin{array}{c} \boldsymbol{OH} + \mathrm{RH} \overset{R3}{\rightarrow} \mathrm{Z_4(nR, nROO)} \overset{R12,R21,R37,R75}{\longrightarrow} \mathrm{nROOH} \overset{R20}{\longrightarrow} \mathrm{nRO} \overset{R25}{\longrightarrow} \mathrm{Z_2(C_2H_5,} \\ \mathrm{CH_3CH_2OO)} \overset{R24,R29,R77,R73}{\longrightarrow} \mathrm{CH_3CH_2OOH} \overset{R42}{\longrightarrow} \mathrm{ethoxy} + \boldsymbol{OH} \end{array}$
	iR Cycle 1
6	OH +RH $\overset{R4}{\rightarrow}$ Z ₅ (iR, iROO) $\overset{R13,R14,R35,R74}{\longrightarrow}$ iROOH $\overset{R17}{\longrightarrow}$ iRO+ OH
	iR Cycle 2
7	$ \begin{array}{l} \boldsymbol{OH} + \text{RH} \xrightarrow{R4} \text{Z}_5(\text{iR, iROO}) \xrightarrow{R13,R14,R35,R74} \text{iROOH} \xrightarrow{R17} \text{R23} \\ \xrightarrow{R19,R26,R39,R72,R81} \xrightarrow{\text{CH}_3\text{OOH}} \xrightarrow{\text{CH}_3\text{O}} \text{CH}_3\text{O} + \boldsymbol{OH} \end{array} $
	iR/primary coupling
8	OH +RH $\stackrel{R4}{\rightarrow}$ Z ₅ (iR, iROO) $\stackrel{R14}{\longrightarrow}$ Z ₄ (nR, O ₂ QOOH ₁) $\stackrel{R11}{\longrightarrow}$ OQ'OOH ₁ + OH
9	OH +RH $\overset{R4}{\rightarrow}$ Z ₅ (iR, iROO) $\overset{R14}{\longrightarrow}$ Z ₄ (nR, O ₂ QOOH ₁) $\overset{R11}{\longrightarrow}$ OQ'OOH ₁ $\overset{R18}{\longrightarrow}$ OQ'O ₁ + OH
10	OH +RH $\overset{R4}{\rightarrow}$ Z ₅ (iR, iROO) $\overset{R14}{\rightarrow}$ Z ₄ (nR, O ₂ QOOH ₁) $\overset{R11}{\rightarrow}$ OQ'OOH ₁ $\overset{R18}{\rightarrow}$ OQ'O ₁ $\overset{R22}{\rightarrow}$ vinoxy $\overset{R27}{\rightarrow}$ CO+ OH

primary catalytic cycle. They are color coded using red. A secondary cycle termed the "iR cycle" emanates from the iR radical and follows paths mP_5 and mP_6 and is color coded using orange and green. The "spur cycle" breaks away from the main cycle via the branching $Z_4(any,nROO) \rightarrow nROOH$ and is coded using blue and yellow. We note there are coupling pathways that connect the cycles. For example, the paths mP8, mP9 and mP10 in Fig. 12, involve reactions such as $iROO+RH \rightarrow iROOH+nR$ that couple the primary and isopropyl cycles. While there are numerous other pathways that have been identified from the data, the 10 pathways are the main production routes for OH during stage 1 of ignition. These reaction pathways emerge automatically from the SOHR method and may be difficult to anticipate without using SOHR. In the following sections we shall discuss and quantify the OH production for each of these cycles.

B. The primary cycle

We compute the efficiency of the primary OH-catalytic cycle as follows. The cycle is initiated by the production of an n-propyl radical (nR) at time t. Then, all carbon tracking pathways emanating from nR are followed until a time $t+\delta$ where δ is selected to be long enough for the chemistry of the cycle to be concluded (typically ~ 0.05 s under present conditions) and the cumulative probabilities are computed. The pathways corresponding to the primary OH cycle of Fig. 1 are

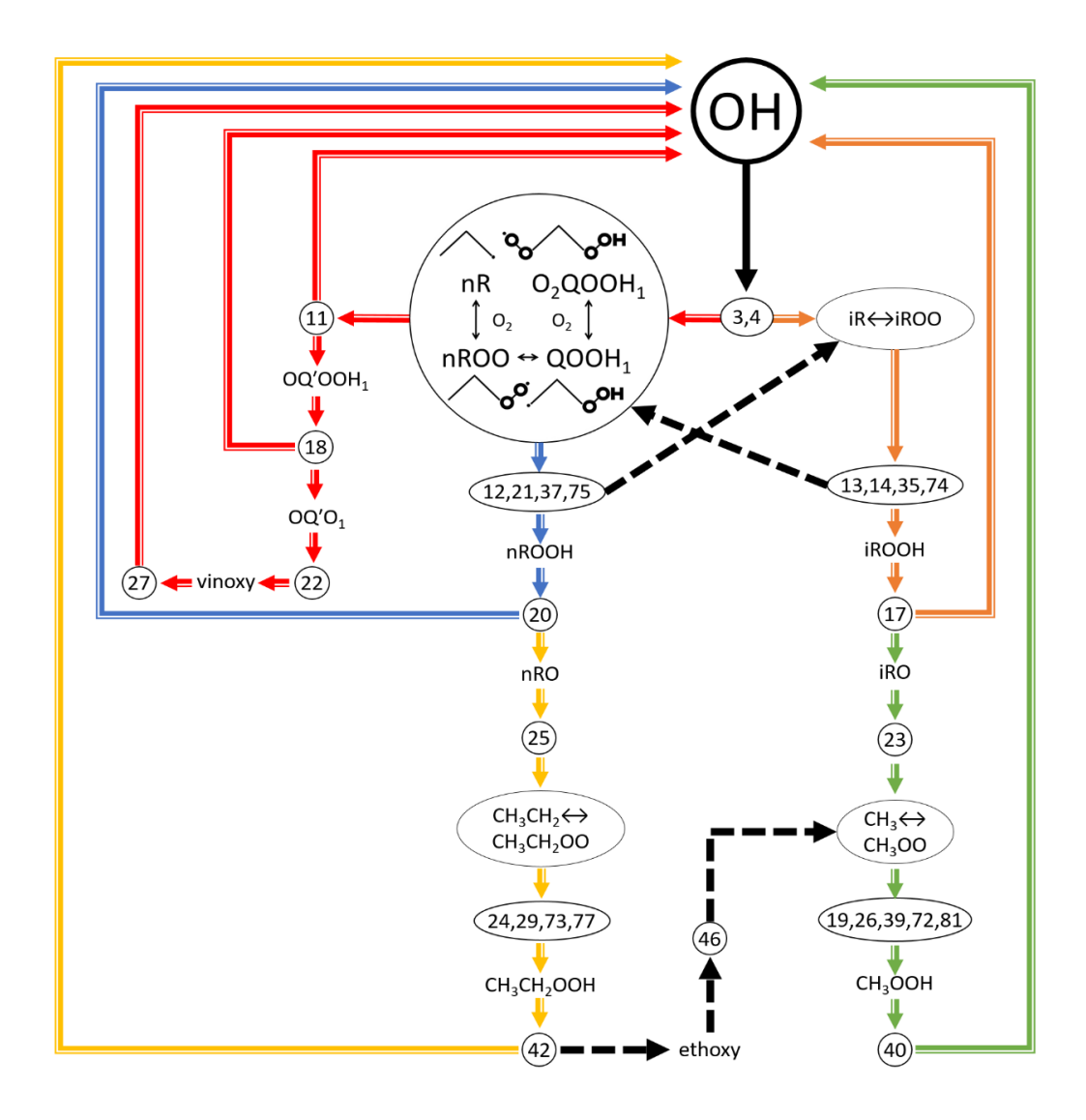


Fig. 13. Catalytic cycles generating OH radical production during propane ignition. The red curves comprise the primary catalytic cycle. The tan and green curves make up the ipropyl cycle. The blue and yellow are the spur cycle that branches off from the primary cycle. The most numerically important pathways constituting these cycles are provided in Table 4. The black dashed lines are reaction routes that couple the cycles together.

the first three listed in Table 4. Following the methodology outlined in Sec. IIC, the cumulative OH-production probability for the three pathways are combined to yield

$$\chi(t, t + \delta) = \chi_1(t, t + \delta) + \chi_2(t, t + \delta) + \chi_3(t, t + \delta) \tag{11}$$

The quantity $\chi(t, t + \delta)$ represents the number of OH-radicals generated from the primary cycle during a time window $[t,t+\delta]$ given that an nR-radical was created at time t. Its maximum possible value is 3.

In Fig. 14 we show $\chi(t, t + \delta)$ as a function of the two variable t and $t + \delta$. The upper panel shows a contour diagram of $\chi(t, t + \delta)$ while the lower panel shows curves obtained by plotting $\chi(t, t + \delta)$ versus δ for various fixed values of t. It is seen that $\chi(t, t + \delta)$ converges quickly as δ increases so that the number of OH-radicals produced is effectively constant when $\delta > 0.05$ s. We note that this δ value is short compared to the ignition time of 0.77 s thus confirming the usual steady state view of chain branching ignition for the primary cycle. The time-dependent OH-production profiles in Fig. 14 are understandable in terms of the pathway theory. The OH radicals are released sequentially, with the first OH produced promptly ($t \sim 10^{-5}$ s) (pathway p1 of Table 4), and the second and third (pathways p2 and p3) are delayed by $t \sim 0.01$ s. The required value of δ for χ_2 and χ_3 is effectively determined by the lifetime of the OQ'OOH₁ species, which is roughly 1.5×10^{-2} s at 650 K. The asymptotic value for the cumulative OH production number, $\lim_{\delta \to \infty} \chi(t, t + \delta)$, strongly depends on initiation time t and reveals a marked decline in the efficiency of the primary cycle with increasing time t. It is seen that about 2.3 OH's are produced from a single nR-radical during early stage 1 of ignition. For later times, and especially during stage 2 of ignition, the production rate from the primary cycle falls off dramatically.

To understand the *t*-dependence of the OH-production $\lim_{\delta\to\infty}\chi(t,t+\delta)$, consider the reactions that comprise the loss mechanisms for the primary cycle. The dominant losses occur through the sink reactions of the group Z₄=(nR, nROO, QOOH₁, O₂QOOH₁). The fractional reaction rates of the sinks of the Z₄ CG are plotted versus time in Fig. 15. At early times, the dominant sink for Z₄ follows the primary cycle, i.e. Z₄(any,O₂Q'OOH₁) \rightarrow OQ'OOH₁+OH, reaction R₁₁ from Table 1. However, for times t>0.5 s we see that loss reaction Z₄(any,ROO) \rightarrow HO₂+propene, reaction R₃₂, takes over as the main sink for Z₄; the pathways that follow this route are found to be ineffective as OH-sources and hence $\lim_{\delta\to\infty}\chi(t,t+\delta)$ declines. It is interesting to note that several peroxy radical recombination reactions, such as nROO+HO₂, nROO+nROO, and nROO+iROO, also play a significant role during the later stages of ignition.

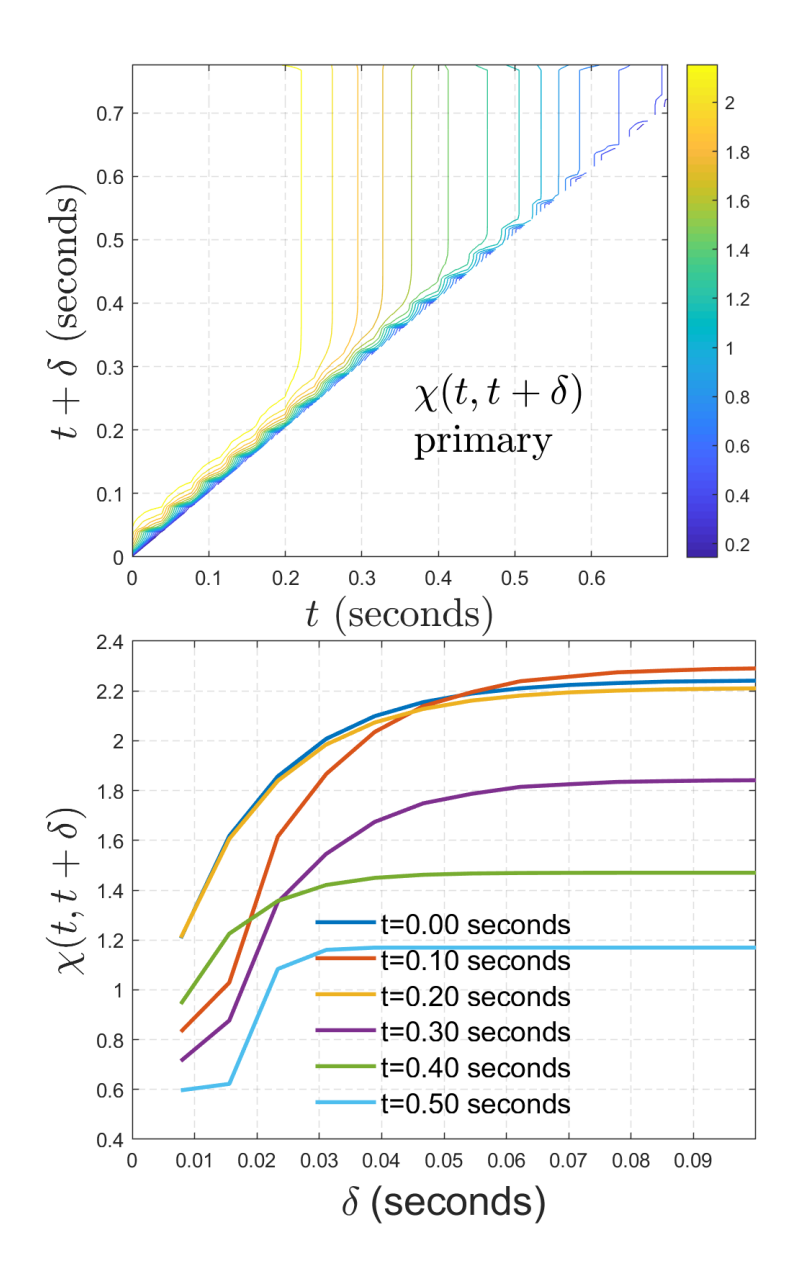


Fig. 14. The cumulative OH production, computed for the three pathways comprising the primary catalytic cycle. The upper panel shows a contour diagram of $\chi(t, t + \delta)$ while the lower panel shows curves obtained by plotting $\chi(t, t + \delta)$ for various fixed values of t. It is seen that $\chi(t, t + \delta)$ converges quickly for t>0.05 s. The curves terminate for $t+\delta > \tau_{ig} = 0.77$ s since the kinetics is not modeled past the full ignition time.

These reactions are found to generate pathways that produce little or slowly emerging OH.

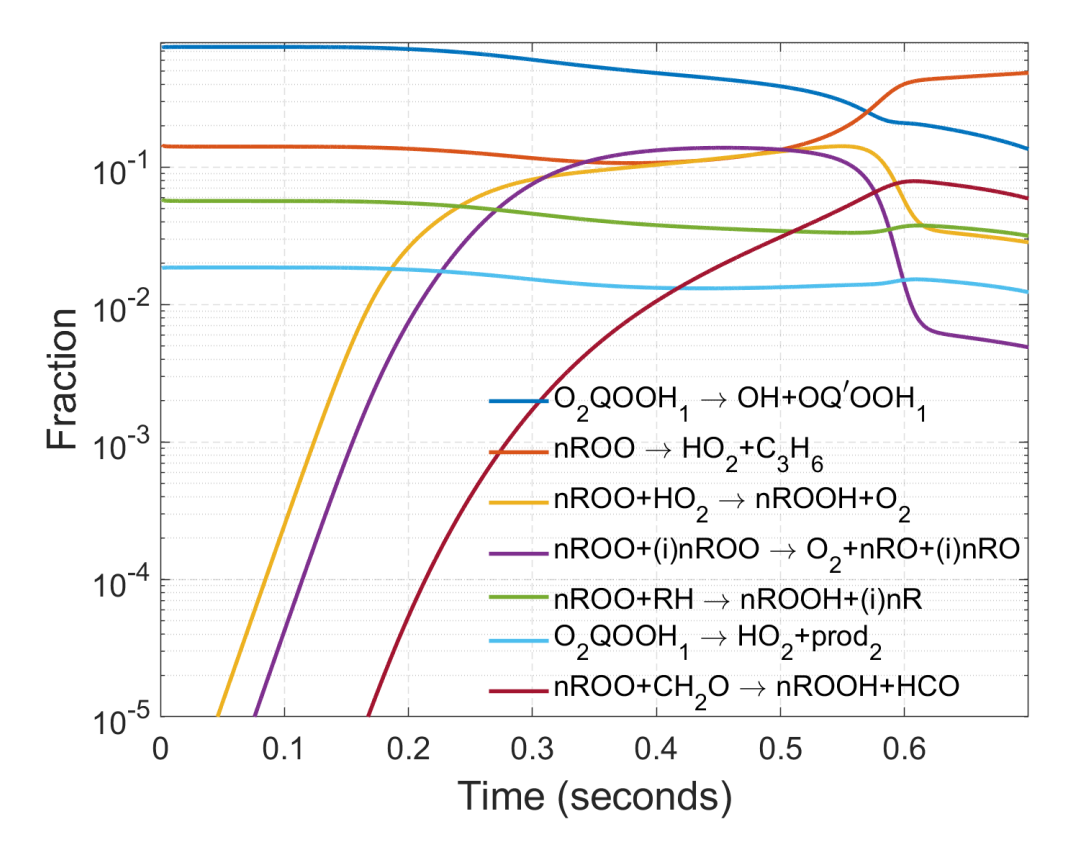


Fig. 15. The rates of sink reaction consuming the Z_4 group expressed as fractions of the total. The fraction indicates the ratio $\omega_i(t)/\sum_j \omega_j(t)$ where $\omega_i(t)$ are the rates of the sink reactions for any member of the CG and sum is over all sink reactions. Note that the important reaction nROO+nROO contains a stoichiometric factor of 2 for Z_4 loss.

While there are experimental and high-level theoretical studies [23,2929,30] characterizing the reactions involved in the primary cycle, there are limited studies on these secondary pathways that deplete the nROO reactive flux. The Merchant *et al.* [24] model relies on estimates for the rate constants for all three secondary processes, nROO+HO₂, nROO+nROO, and nROO+iROO. There are no direct studies on the nC₃H₇OO+HO₂ reaction. However, the limited experimental and theoretical studies [58-60] at T < 400 K on the analogous $C_2H_5OO+HO_2$ reaction seem to indicate that this reaction proceeds on the triplet surface to form O_2 and C_2H_5OOH as the dominant products with rate constants that exhibit a weaker negative-T dependence than the estimate used in the model [2424] for nC₃H₇OO+HO₂. Unlike the nROO+HO₂ reaction system, there are some limited

low-temperature (T < 400K) studies for the self-reactions of the propylperoxy radicals. The Merchant et al. [24] model asumes the same rate constants for the self-reactions and cross-reactions between the two i,n-propylperoxy radicals. While the rate constant estimate used in the model for nC₃H₇OO+ nC₃H₇OO is in reasonable agreement with the recommendation from Atkinson et al. [58], literature studies indicate that the iC₃H₇OO+ iC₃H₇OO reaction proceeds at a rate that is about a factor of 300 slower than the nC₃H₇OO+ nC₃H₇OO reaction. With these known rate constants for the self-reactions of the two propylperoxy radicals, one can conjecture that the rate constants for the cross-reaction (nC₃H₇OO+ iC₃H₇OO) will be lower than the nC₃H₇OO+ nC₃H₇OO rate constant. Lastly, for these peroxy radical self-reactions, the Merchant et al. [2424] model includes only one product channel that forms two propoxy radicals and O2, whereas the room-temperature kinetic studies indicate the formation of an additional and equally important channel forming two stable products, (an alcohol and an aldehyde or ketone) and O₂. Recent studies [29,30] also seem to suggest the relevance of this additional product channel to explain the formation of the observed alcohol and aldehyde/ketone intermediates in low temperature propane oxidation. Higher temperature experimental studies (or alternately theoretical studies) are recommended for these reactions given that these emerge as important secondary channels from the present analysis.

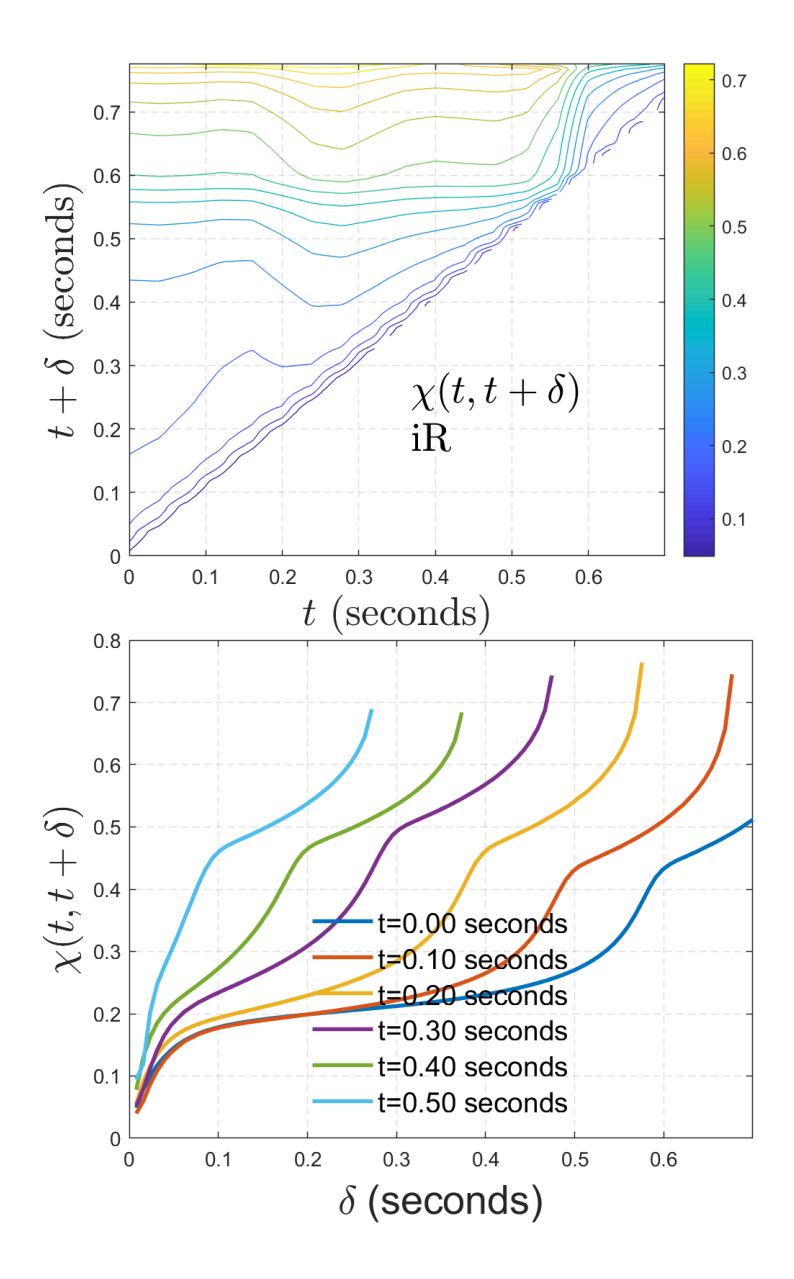
C. The isopropyl cycle

The ipropyl cycle is initiated by the formation of an iR radical as seen in Fig. 13. The first branch of the ipropyl cycle (shown in tan on Fig. 13) is OH+RH $\stackrel{R4}{\rightarrow}$ Z₅(iR, iROO) $\stackrel{R13,R14,R35,R74}{\longrightarrow}$ iROOH $\stackrel{R17}{\longrightarrow}$ iROO+OH. Thus, this path creates the CG Z₅ which forms the isopropyl-hydroperoxide iROOH through one of four possible H-abstraction reactions. A second OH-radical (green) is generated following the iRO species further, i.e. OH+RH $\stackrel{R4}{\rightarrow}$ Z₅(iR, iROO) $\stackrel{R13,R14,R35,R74}{\longrightarrow}$ iROOH $\stackrel{R17}{\longrightarrow}$ iROOH $\stackrel{R23}{\longrightarrow}$ Z₁(CH₃, CH₃OO) $\stackrel{R19,R26,R39,R72,R81}{\longrightarrow}$ CH₃OOH $\stackrel{R40}{\longrightarrow}$ CH₃OO+OH. The iRO fragment, generated by the first OH production, is seen to undergo a unimolecular dissociation to yield a methyl radical CH₃. The CH₃ is part of a CG Z₁ =(CH₃,CH₃OO) with CH₃OO that experiences a further abstraction reaction to form CH₃OOH. This methyl hydroperoxide molecule dissociates to form OH and methoxy. Hence, the ipropyl cycle can yield up to two OH-radicals. Unfortunately, there are no direct studies of the rates of the high barrier iROO+RH abstraction

reaction. Such studies would be quite useful since this is a key step yielding iROOH, which in turn generates OH.

The efficiency of the iR catalytic cycle is again assessed using the cumulative OHproduction probability $\chi(t,t+\delta)$ which is now computed using a sum over pathways included in the iR cycle. The most important iR paths are given in Table 4, but additional pathways are included that follow some of the less probable products of iRO and Z_1 . The quantity $\chi(t, t+\delta)$ is the number of OH radicals generated by following the chemistry of a single iR radical at time t for a time window δ . In Fig. 16, a contour diagram of $\chi(t, t + \delta)$ is provided in the upper panel while in the lower panel a series of curves of $\chi(t, t + \delta)$ versus δ are shown for various values of t. Several features are evident from the plot. First, the net OH production of the iR cycle is significantly lower than the primary cycle during stage 1 of ignition, yielding only about 0.2-0.3 OH's per cycle. The contribution significantly increases during stage 2, where 0.6 OH's per cycle are produced. Also, we see a strong time dependence in the production rate, i.e. 0.2 OH's are produced promptly (in less than 0.1 s) and further OH's are delayed requiring over 0.2 s). The origin of this effect can be easily traced to the pathways themselves. The prompt OH production comes from the decay of iROOH(→OH+iRO); the rate limiting step along these pathways is iROOH dissociation itself, which occurs with a lifetime of about 0.023 s at 650K. The delayed OH production is traced to pathways that involve dissociation of CH₃OOH and C₂H₅OOH which are generated from the subsequent iRO chemistry. The lifetimes of CH₃OOH and C₂H₅OOH at 650K are much longer than iROOH, roughly 0.26 s and hence the appearance of OH is delayed. The temperature rise at the first ignition threshold also induces the reservoir of CH₃OOH and C₂H₅OOH to dissociate. Finally, as with the primary cycle, the asymptotic value of the height of the cumulative OH production probability, $\lim_{\delta \to \infty} \chi(t, t + \delta)$, strongly depends on t. However, unlike the primary cycle for which the asymptote decreased with increasing t (see Fig. 14), for the iR cycle the asymptote increases at longer times. This reflects the onset of new pathways (i.e. those yielding CH₃OOH and C₂H₅OOH) and the subsequent decay of those compounds into OH-radicals.

Further insight into the iR cycle is obtained by considering the relative importance of the decay mechanisms of the Z_5 CG (iR,iROO). In Fig. 17 fractional rates of various depletion reactions of Z_5 are plotted versus time. It is seen that early in the ignition process, t<0.2 s, the primary Z_5 sink reactions are iROO \rightarrow HO₂+propene and iR+O₂ \rightarrow propene+HO₂ which are



Fig, 16. The cumulative OH production $\chi(t, t + \delta)$ for the ipropyl (iR) cycle which is the number of OH radicals generated by following the chemistry of a single iR radical created at time t for a time window δ . The contour diagram in the upper panel and the curves in the lower panel reveal a fairly strong δ dependence of the results.

effectively terminations for the OH-radical. The iROO+RH→iROOH+i(n)R pair of reactions occurs with about a 7% efficiency and lead to the prompt production of OH. At later times the HO₂

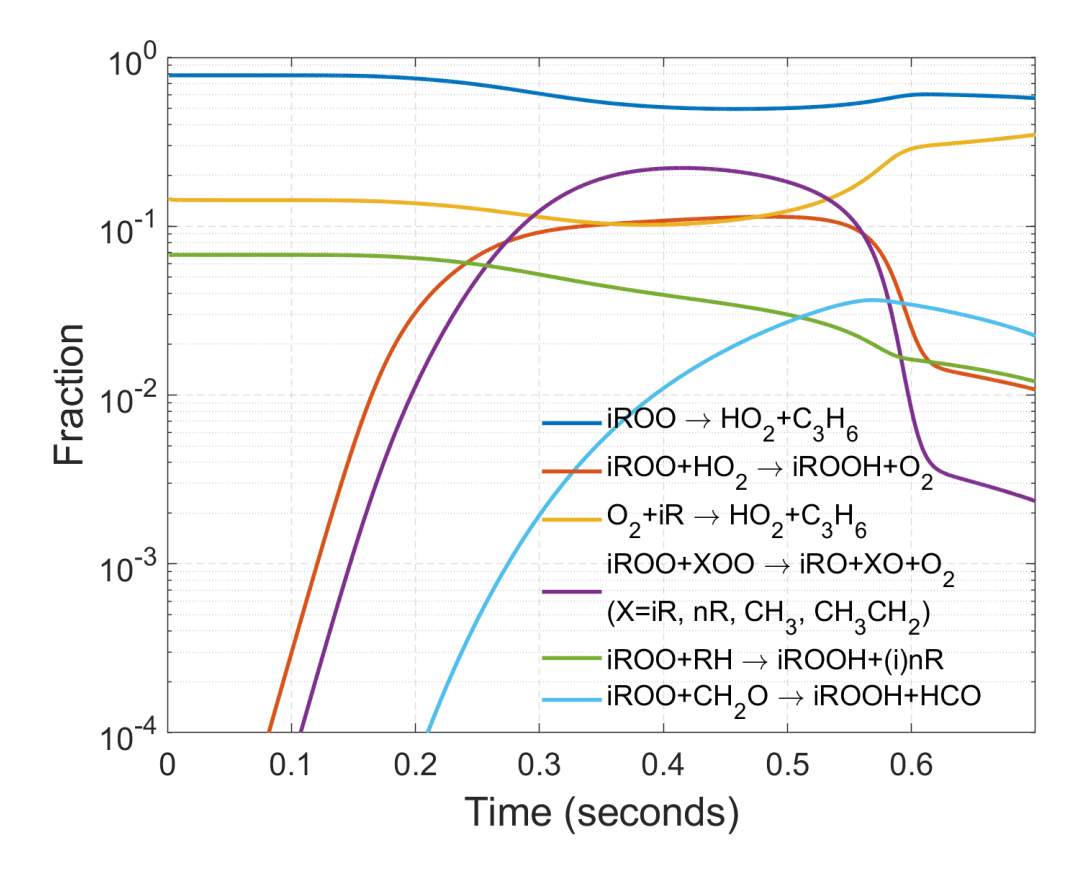


Fig. 17. The rates of sink reaction consuming the group $Z_5 = (iR,iROO)$ expressed as fractions of the total. The fraction indicates the ratio $\omega_i(t)/\sum_j \omega_j(t)$ where $\omega_i(t)$ are the rates of the sink reactions for any member of the CG and sum is over all sink reactions.

reaction, iROO+HO₂ \rightarrow iROOH+O₂, and CH₂O reaction, iROO+CH₂O \rightarrow iROOH+HCO, become important Z₅ sinks and iROOH sources.

D. The spur cycle

Another secondary catalytic cycle is provided by the spur cycle (the blue and yellow paths in Fig. 13) which follows a loss pathway from the primary cycle. This is a reaction route that splits off from the primary cycle due to a branching step of the Z₄ CG, i.e. $OH+RH \xrightarrow{R3} Z_4(nR, nROO) \xrightarrow{R12,R21,R37,R75} nROOH \xrightarrow{R20} nRO+OH$. The nRO₂ species abstracts a hydrogen from one of four possible "donor" species to form the long lived nROOH. This spur cycle can potentially

generate two further OH radicals, first through

OH+RH
$$\xrightarrow{RS}$$
 Z₄(nR, nROO) $\xrightarrow{R19,R24,R29,R77,R73}$ CH₃CH₂OOH $\xrightarrow{R42}$ ethoxy+ OH and then the sequential process

OH+RH $\xrightarrow{R3}$ Z₄(nR, nROO) $\xrightarrow{R12,R21,R37,R75}$ nROOH $\xrightarrow{R20}$ nRO $\xrightarrow{R25}$ Z₂(C₂H₅, CH₃CH₂OO) $\xrightarrow{R24,R29,R77,R73}$ CH₃CH₂OOH $\xrightarrow{R42}$ ethoxy $\xrightarrow{R46}$ Z₁(CH₃, CH₃OO) $\xrightarrow{R19,R26,R39,R72,R81}$ CH₃OOH $\xrightarrow{R40}$ CH₃O+ OH . Additionally, there are several less important "direct reaction" pathways that break away from the primary cycle such as OH +RH $\xrightarrow{R3}$ Z₄(nR, nROO) $\xrightarrow{R53}$ propoxide+ OH and OH +RH $\xrightarrow{R3}$ Z₄(nR, nR) $\xrightarrow{R50}$ propoxide+ OH

The efficiency of the spur catalytic cycle is again assessed using the cumulative OHproduction probability $\chi(t,t+\delta)$ which is now computed using a sum over pathways included in the spur cycle. The two most important spur paths are given in Table 4, although the full calculation includes some less probable reactions subsequent to the appearance of the nROOH intermediate. The quantity $\chi(t,t+\delta)$ is the number of OH radicals generated during a time window $[t,t+\delta]$ by following the chemistry of a single nROOH that dominantly comes from nROO+RH at early times and nROO+HO₂ or nROO+CH₂O at later times. The $\chi(t,t+\delta)$ obtained using the SOHR method is shown in Fig. 18. There is a prompt creation of about 0.12 OH radicals during the early stage 1 ignition, and a much larger 0.4-0.5 OH creation that occurs at the stage 1 ignition threshold. The prompt OH is from the direct dissociation of nROOH, while the delayed OH release is traced back to the breakdown of the CH₃OOH and C₂H₅OOH molecules, which is accelerated by the temperature rise at the first ignition threshold. The chemistry of the secondary peroxy radical CH₃OO, which is the precursor to CH₃OOH, is better understood by considering the sink reactions that govern the disposition of the CG Z₁=(CH₃,CH₃OO), which are depicted in Fig. 19. At early times, Z₁ reacts almost exclusively with propane, RH, to yield CH₃OOH. At later times, Z₁ reacts with HO₂ or CH₂O to form CH₃OOH.

E. The multi-cycle catalytic efficiency

As noted above, the OH production efficiency γ of a given catalytic cycle depends on two quantities α and χ via

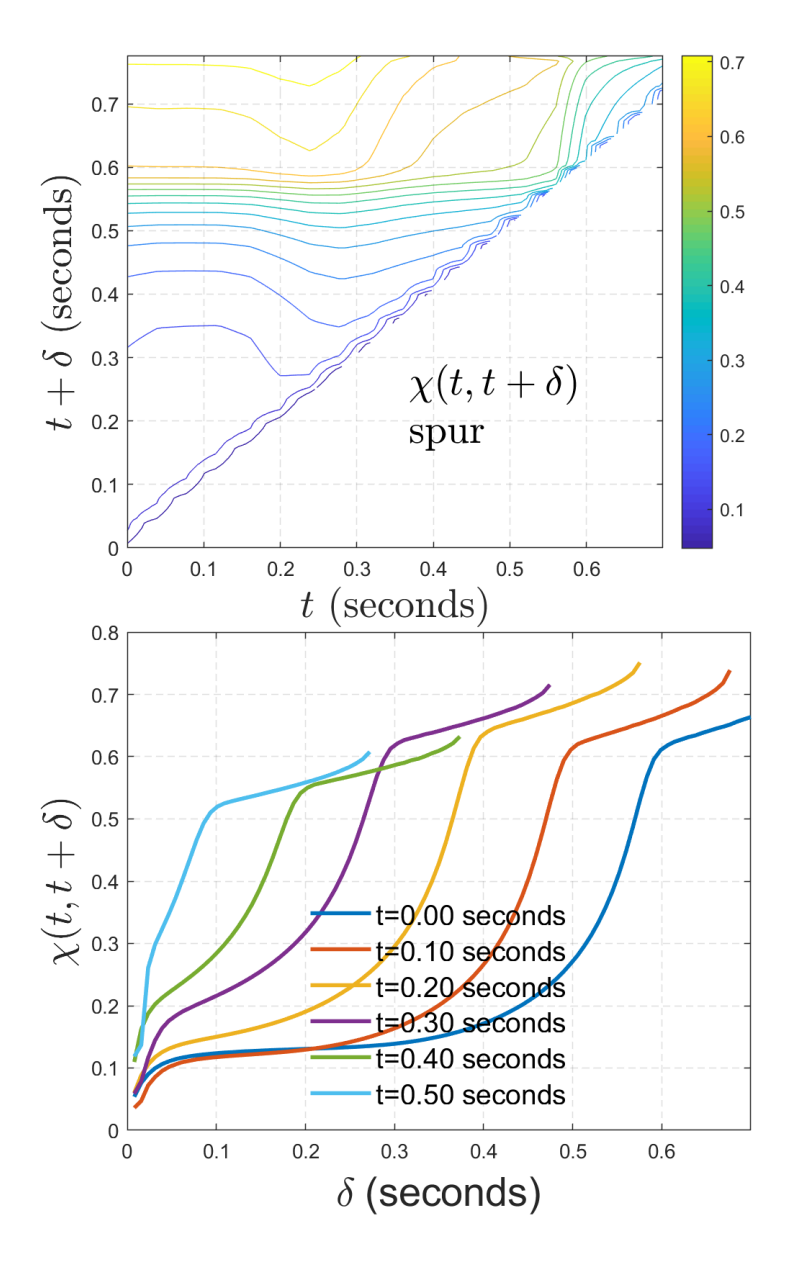


Fig. 18. The cumulative OH production $\chi(t, t + \delta)$ for the spur cycle which is the number of OH radicals generated by following the chemistry of a single nROOH molecule created at time t for a time window δ . The contour diagram in the upper panel and the curves in the lower panel reveal a fairly strong δ dependence of the results.

$$\gamma(t, t + \delta) = \alpha(t) \cdot \chi(t, t + \delta) - 1 \tag{12}$$

Using SOHR we have obtained $\chi(t, t + \delta)$ which is the number of OH-radicals generated during

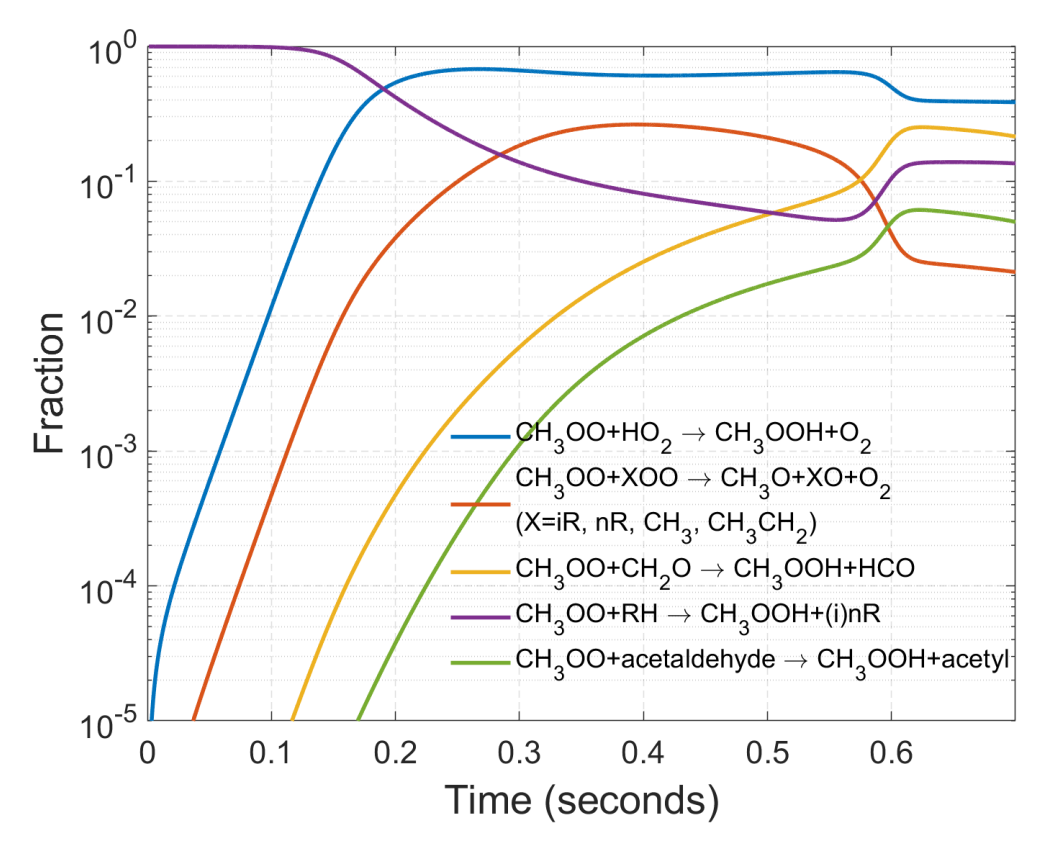


Fig. 19. The rates of the sink reaction consuming $Z_1 = (CH_3, CH_3OO)$ expressed as fractions of the total. The fraction indicates the ratio $\omega_i(t)/\sum_j \omega_j(t)$ where $\omega_i(t)$ are the rates of the sink reactions for any member of the CG and sum is over all sink reactions. It is seen that the H-atom dominant donor species changes from propane (RH), to HO₂, to CH₂O as time progresses.

a cycle from a given nR or iR radical, which initiates the primary, spur, and iR catalytic cycles (nR for primary and spur cycle, iR for the iR cycle). The quantity $\alpha(t)$ is the probability that a OH-radical will react with the mixture to form an nR or iR and thus re-initiate the cycle. Since OH has an ultrashort chemical lifetime of roughly 10^{-8} s, this quantity is given by the instantaneous branching fraction of OH reactions that yield (for nR or spur), $\alpha(t) = \omega(RH + OH \rightarrow nR + H_2O)/\sum_j \omega_j (all OH rxns)$ or for iR $\alpha(t) = \omega(RH + OH \rightarrow iR + H_2O)/\sum_j \omega_j (all OH rxns)$. While SOHR gives exact pathway probabilities, the choice for the value δ to be used depends on the physical interpretation. For the primary cycle, all the OH radicals are produced promptly and we can set $\chi(t, t + \delta)$ to its limiting value, $\lim_{\delta \to \infty} \chi(t, t + \delta) \equiv \chi(t)$. The iR and spur cycles involve

both prompt and delayed production of OH. The delayed production is due to slow CH₃OOH and C₂H₅OOH dissociation accelerated by the temperature jump at the first ignition threshold. Since the delayed OH release is more the result of the ignition rather than its cause, we choose a fairly small time, δ =0.1 which mostly captures the prompt OH release. With the δ value thus set, we define the overall catalytic efficiency to be the sum over cycle contributions

$$\gamma(t) = \sum_{i}^{cycles} \alpha_{i}(t) \chi_{i}(t) - 1$$
 (13)

In Fig. 20, we plot the contribution to $\gamma(t)$ from various catalytic cycles. The full (exact) result, is shown with the dashed line. This exact result is converged using all of the 119 identified pathways that serve as sources of OH. It is seen that the primary cycle is the largest OH

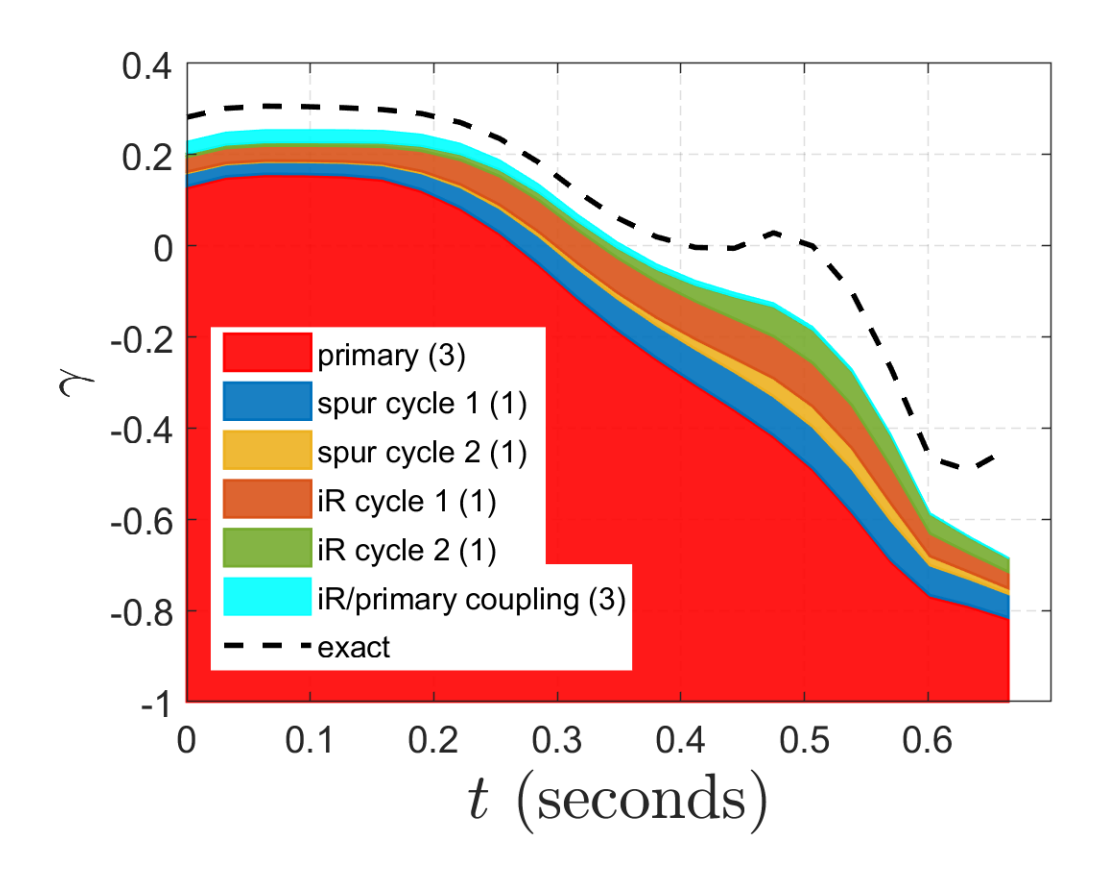


Fig. 20. The catalytic efficiency $\gamma(t)$ for various cycles as a function of time for T=650 K and p=10 bar. The individual pathway contributions are shown with the color shading. The number in parenthesis indicates the number of pathways for each cycle. The exact result is from all 119 identified OH producing paths that agrees with the result of conventional kinetic simulation.

production mechanism and contributes roughly 88% of the OH production during the early stages of ignition. During the second ignition stage, the efficiency of the primary cycle falls off significantly and less than half of the OH production occurs through this route. The iR and spur cycles (and their coupling) account for about 2/3 of the remaining OH generation during first stage ignition. Thus, about 95% of the OH production during stage 1 ignition can be accounted for using the chemistry summarized in Fig. 13. The remaining production probability is broadly distributed over 109 SOHR pathways and includes a large contribution from H_2O_2 dissociation. It is seen that the root of $\gamma(t)=0$ provides an approximate estimate of the location of the first ignition threshold that occurs at 0.55 s.

It is interesting to compare the exact catalytic efficiency obtained by SOHR with the simpler approximate results obtained using snapshot steady state products of branching ratios. In Fig. 21 we show the approximate and exact results for the primary cycle which account for most of the first stage OH-production. The approximate result shown is obtained using the expressions

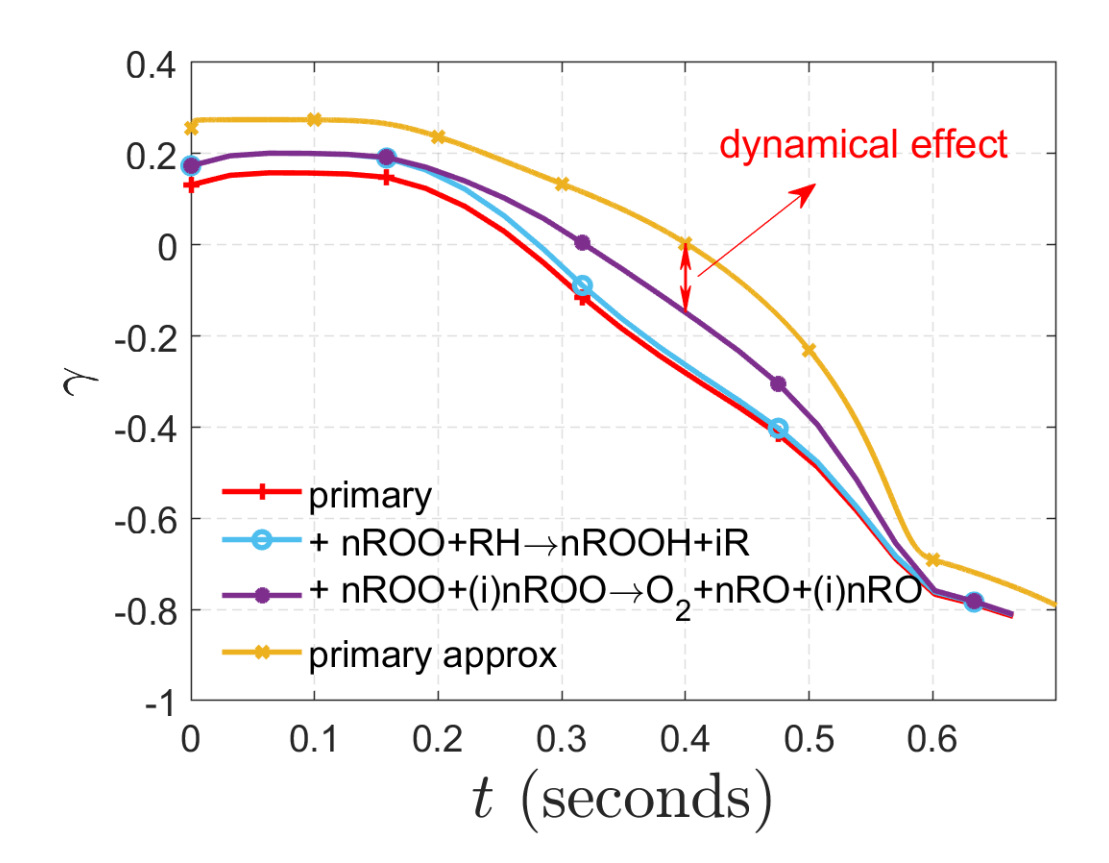


Fig. 21. The catalytic efficiency $\gamma(t)$ for the primary cycle only as a function of time for T=650 K and p=10 bar. The exact $\gamma(t)$ (red curve) computed from paths 1-3 using SOHR and the approximate result (gold) obtained using only the loss terms from reactions 37, 41, and 75 similar to eqs. 27-29 of ref. 24. The blue and purple curves show the modification to the exact (SOHR) result if the nROO+RH and nROO+(i)nROO sink terms (not included in ref. [24]) are omitted from the SOHR calculation. The remaining difference is due to dynamical effects.

introduced in ref. 24 while the exact result is obtained from the three contributing chemical pathways mP1-mP3. It is seen that there is a reasonable agreement between the two levels of theory although the differences grows to about 25% at t=0.4 s. The source of difference between the two theories can be traced to two factors. irst, certain sink (loss) terms are neglected in the approximate expression, viz. the reactions nROO+RH \rightarrow ROOH+iR and nROO+(i)nROO \rightarrow O₂+nRO+(i)nRO. As shown in the figure, when these sink terms are eliminated from the SOHR pathways, the catalytic efficiency is shifted upward toward the approximate expression. The remaining difference is dominantly a dynamical effect leading to, e.g., the breakdown of the steady state approximation for the OQ'OOH₁ species. Nevertheless, we note that the approximate expression is useful in the analysis of the primary cycle. However, the steady state approximation is much less useful for the other catalytic cycles in the problem.

F. Temperature Dependence

The analysis of propane low temperature ignition presented above has focused on the reaction conditions of T₀=650 K and P₀=10 bar. For these initial values, the ignition event is a two stage process occuring on a time scale of roughly 1 s. It is of interest to assess the sensitivity of the ignition chemistry to the initial conditions. While we have not made an exhaustive study of the ignition chemistry versus T and P, we have considered several other cases. As temperature is lowered, the ignition delay time exponentially increases. This reflects the activation threshold for several OH producing dissociation processes such as those for the ketohydroperoxides. At 550 K and 10 bar, e.g., the ignition delay time has grown to approximately 60 s while at 500 K and 10 bar it has gone up to about 1800 s. Furthermore, at lower temperatures many of the manifestations of multiple stage ignition have disappeared and the chemical evolution of the mixtures is significantly modified. Figures 22 and 23 show the production mechanisms of OH radicals versus

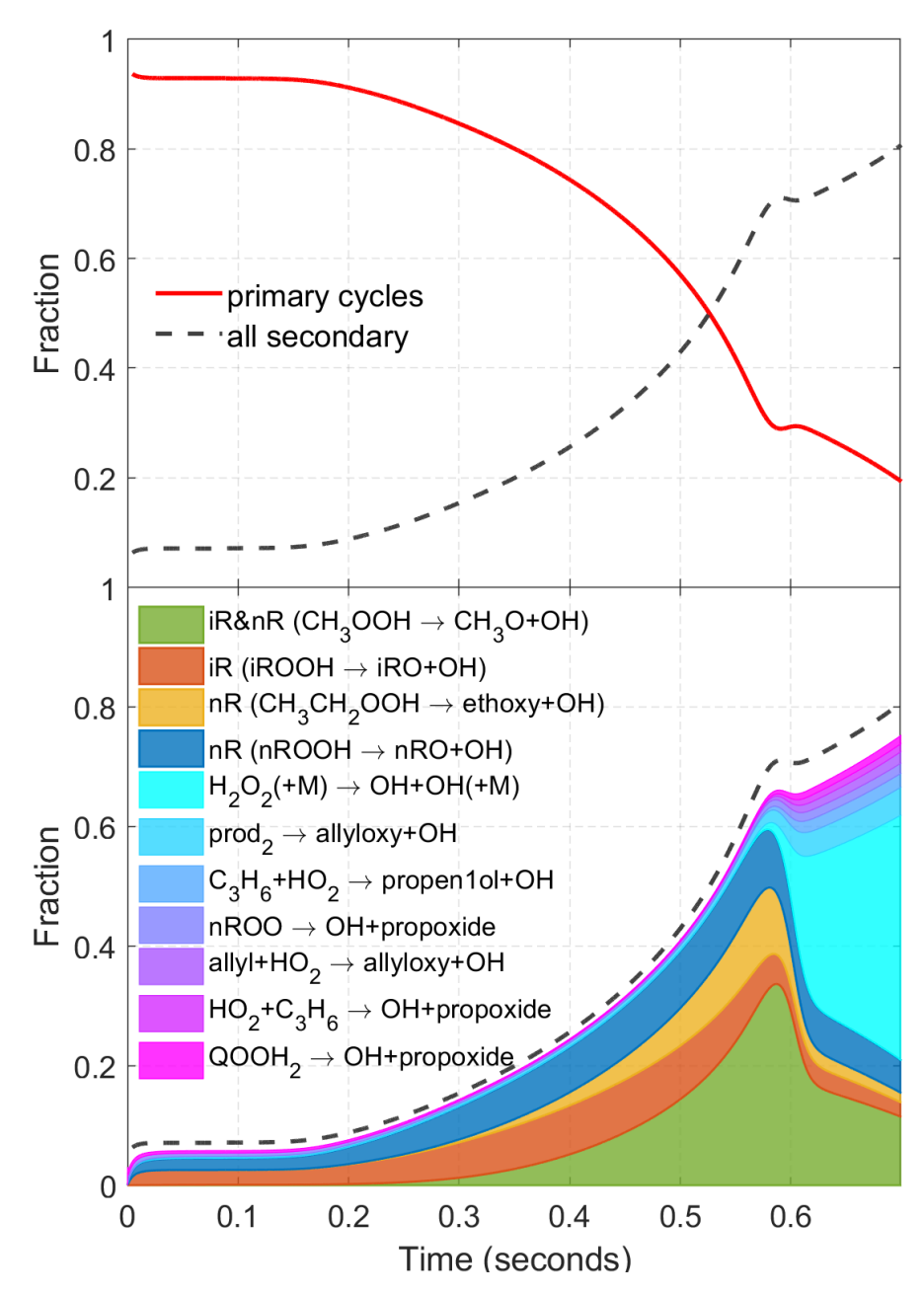


Fig. 22. Contribution of various production pathways for the creation of OH-radicals during propane ignition at 650 K and 10 bar. In the upper panel, the fractional contribution of the primary cycle to the OH production rate versus time is shown in red while the secondary mechanisms shown with the dashed line. In the lower panel, the contributions of various secondary mechanisms are labeled by the last (OH producing) reaction along the path. The processes are labeled by the final (OH-producing) reaction of the mechanisms. The first four paths correspond to the iR and spur cycles shown in Fig. 13.

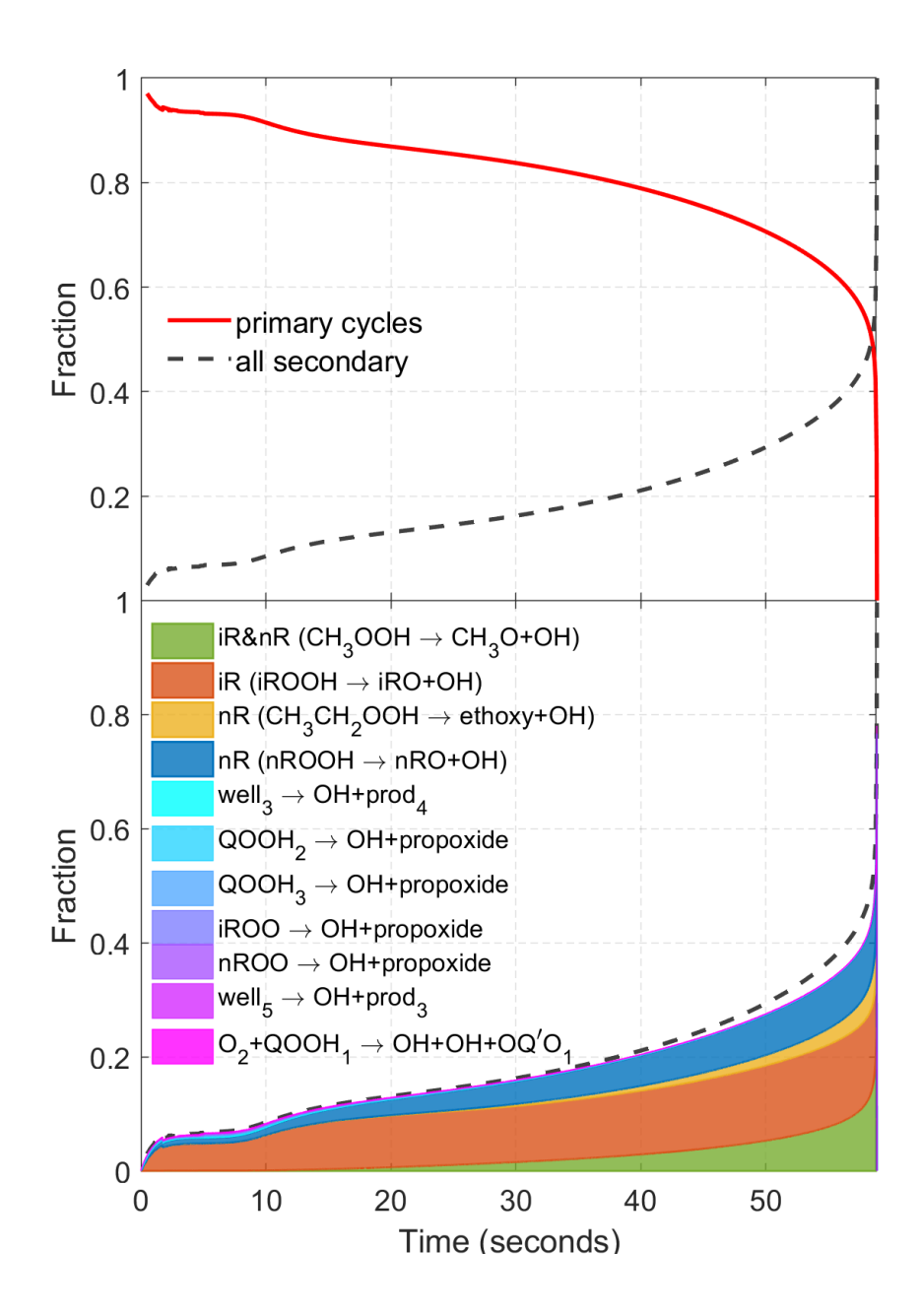


Fig. 23. The same as Fig. 22 except for the initial conditions T=550 K, p=10 bar and ϕ =1.0.

time at 650 K and 550 K, respectively. In the upper panels, we show the instantaneous fraction of OH production due to the three pathways of the primary cycle and the remaining fraction due to all other identified secondary mechanisms. While the secondary chemistry greatly outstrips the primary chemistry during the second ignition stage at 650 K, at 550 K the primary cycle remains significantly larger until the ignition threshold. Furthermore, the detailed secondary mechanisms

are significantly different quantitatively in the two cases. In the lower panels of Figs. 22 and 23, the secondary chemistry is decomposed into various OH production cycles that are labeled by the final reaction step that produces the OH. As discussed previously, at 650 K the chemistry of the iR and spur cycles comprise most of the secondary OH production during the first ignition stage but a plethora of additional pathways develop during the second stage. In Fig. 22, we see that during stage two less than 1/3 of the secondary OH production occurs through the iR and spur mechanisms while new paths leading to H₂O₂ dissociation and passing through other QOOH isomers start playing a large role. In contrast, we see in Fig. 23 that the secondary chemistry at 550 K remains dominated by the four pathways of the iR and spur cycles up to the ignition threshold. Hence, the lower temperature ignition chemistry remains "simple" and quantitatively describable by the reaction routes depicted in schematic of Fig. 13.

VII. Conclusions

In this work we have illustrated how the SOHR method can be usefully employed to analyze the chemistry of a realistic hydrocarbon combustion problem. Although the mechanism is large, it was demonstrated that concentrations of any species could be calculated using a relatively small number of chemical pathways. The construction chattering groups (CG) of species was introduced to facilitate treatment of problems with separation of timescales in which long repeating (or chattering) pathways occur to establish quasi-equilibrium states. The CG is similar to a lumped set of species but is computationally adapted for pathway analysis. The key advantage of the SOHR method is that it provides an "exact" means to identify and quantify complete chemical pathways that develop during the evolution of complicated kinetic networks. This capability can be used to deconstruct kinetic observables into quantitative contributions from multistep chemical mechanisms, i.e. chemical pathways. In the present study, we have employed this tool to understand the chemistry underlying the low temperature autoignition of propane/air mixtures. The auto-catalytic cycles involving the highly reactive OH radical could be identified through chemical pathways that begin with the attack of an OH radical on a species and end with the generation of secondary OH product(s). The primary cycle, involving the n-propyl radical and its subsequent oxidation through QOOH₁ and ketohydroperoxide intermediates, was found to account for 88% of the OH generation early in the ignition process for T=650 K. However, the during the latter phases of stage 1 ignition and for all of stage 2 ignition the primary cycle fell off dramatically

in quantitative importance. However, several important secondary OH production cycles were identified that could then account for most of the OH production during the entirety of stage 1 ignition. During stage 2 ignition the number of required pathways became much larger as the role of secondary reactions increased in importance. While the OH production rates were converged using the SOHR pathway expansion during stage 2 ignition, the large number of paths (119) made the physical interpretation difficult. It is interesting to note, however, that the homogeneous autoignition chemistry at even lower temperatures (e.g. 550K) proved to be actually simpler and well described using the small number of chemical pathways summarized in Fig. 13.

Essential to the generation of OH radicals from the secondary cycles (the iR and spur cycles in particular) is the formation of closed shell hydroperoxide species, iROOH, nROOH, CH₃OOH, and C₂H₅OOH. These molecules are generally produced via reaction of an "acceptor" peroxy radical (iRO₂, nRO₂, CH₃OO, or C₂H₅OO) with a hydrogen-atom "donor" species (CH₂O, HO₂, and propane), see the schematic in Fig. 24. Each of the acceptor species is part of a CG with a precursor radical (iR, nR, CH₃, or C₂H₅) that undergoes rapid association/dissociation

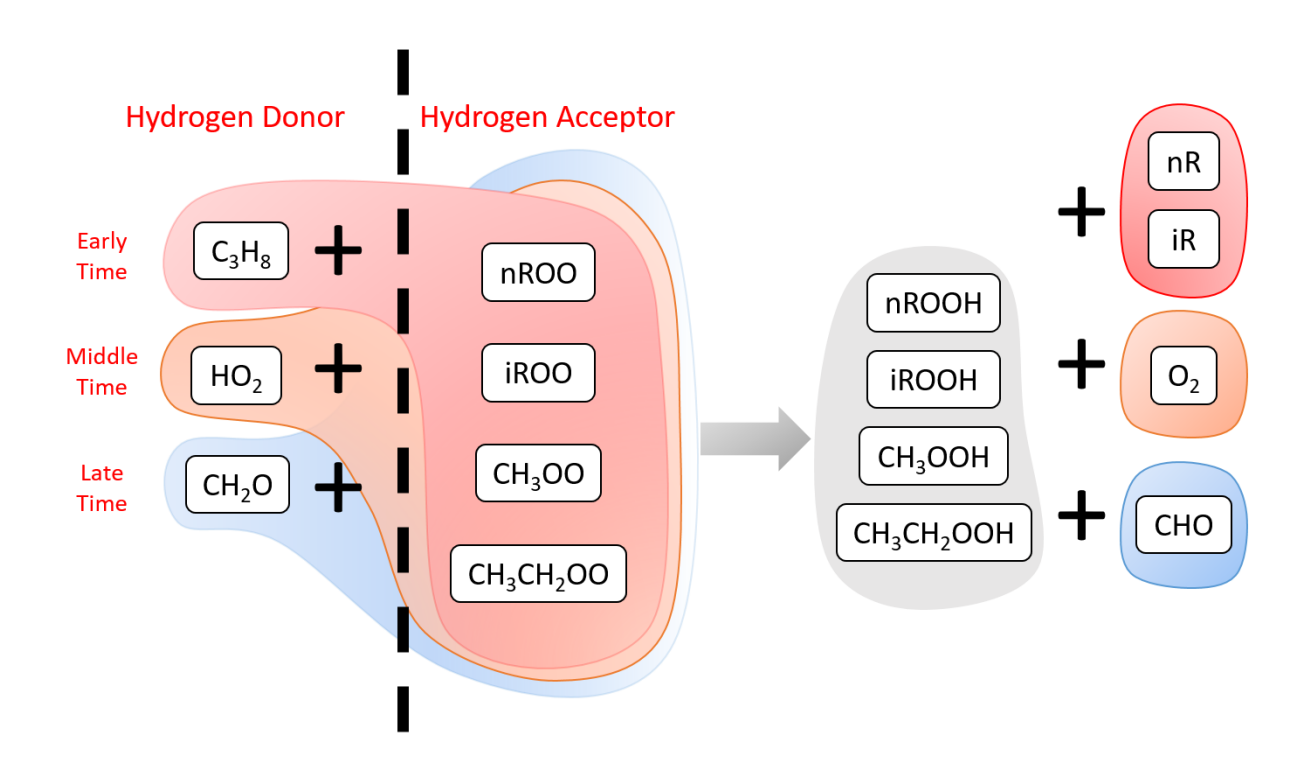


Fig. 24. A schematic diagram showing the reactions that generate important hydroperoxyide molecules from peroxy radicals (acceptors) reacting with C₃H₈, HO₂, or CH₂O (donors). The dominant donor species for short, medium, and long times is indicated.

with O₂. The fractional rates of these H-atom abstraction reactions depend on the concentration of the H-atom donor species. For each acceptor species, the dominant H-atom donor at early times is propane, at intermediate times is HO₂, and at long times is CH₂O. The ordering reflects the concentration growth of HO₂ and CH₂O and the decline of that for C₃H₈ as a function of time.

We have also noted that several previously under appreciated reactions have a noticeable effect on the efficiency of the primary OH production cycle. Specifically, the peroxy radical self reactions $nROO+(i)nROO \rightarrow O_2+nRO+(i)nRO$ can act as a significant sink reaction for the group Z₄, and hence a loss term for the primary cycle. As mentioned earlier, these reactions were studied over 30 years ago [58,61] over limited experimental temperature ranges relevant to atmospheric chemistry. It may be of some current interest to attempt a high quality *ab initio* treatment of these reactions to properly characterize the temperature dependence and additional product channels that can emerge at conditions relevant to combustion.

Finally, we also point out that the SOHR method has application to the combustion problem beyond identifying and quantifying catalytic cycles. For example, we have also begun to explore the use of SOHR pathways as a means to construct reduced chemical mechanisms. A reduced mechanism would consist of a model with a small number of species and reactions capable of reproducing the essential chemistry of the full mechanism. Using the chemical pathways generated by SOHR, we can locate the major routes by which the chemistry occurs, and the portions of the mechanism that are rarely visited. This work is complementary to the methodology of Lu and Law [48] that employ the directed relation graph method to simplify chemical mechanisms.

Acknowledgements

This work was supported by the National Science Foundation through grant CHE1556041. The work of MJD and RS was supported by the U. S. Department of Energy, Office of Basic Energy Sciences, Division of Chemical Sciences, Geosciences, and Biosciences, under Contract No. DE-AC02-06CH11357.

Supplementary Material

Figures S1, S2, and S3 showing the convergence of [CO], [CH₂O], and [C₃H₆] as a function of the number of pathways.

REFERENCES

[1] C. K. Westbrook, Chemical kinetics of hydrocarbon ignition in practical combustion systems, Proc. Combust. Inst. 28 (2000) 1563-1577.

[2] J. A. Miller, R. J. Kee, and C. K. Westbrook, Chemical Kinetics and Combustion Modeling, Annu. Rev. Phys. Chem. 41 (1990) 345-387.

[3] H. J. Curran, P. Gaffuri, W.J. Pitz, and C. K. Westbrook, A Comprehensive Modeling Study of n-Heptane Oxidation, Combust. Flame 114 (1998) 149-177.

[4] C. K. Law, Combustion Physics, Cambridge University Press, 2006.

[5] A. Saltelli, K. Chan, E. Scott, Sensitivity Analysis, John Wiley, Chichester, NY, 2000.

[6] T. Turanyi, Sensitivity analysis of complex kinetic systems. Tools and applications, J. Math. Chem. 5 (1990) 203–248.

[7] J. J. Scire, F. L. Dryer, R. A. Yetter, Comparison of global and local sensitivity techniques for rate constants determined using complex reaction mechanisms, Int. J. Chem. Kin. 33 (2001) 784-802.

[8] T. Ziehn, A. S. Tomlin, A global sensitivity study of sulfur chemistry in a premixed methane flame model using HDMR, Int. J. Chem. Kin. 40 (2008) 742-753.

[9] R. T. Skodje, A. S. Tomlin, S. J. Klippenstein, L. B. Harding, M. J. Davis, Theoretical validation of chemical kinetic mechanisms: combustion of methanol. J. Phys. Chem. A 114 (2010) 8286-8301.

[10] T. Turanyi, A. S. Tomlin, Analysis of Reaction Mechanisms, Springer, Berlin Heidelberg, 2014.

[11] H. Wang, D. A. Sheen, Combustion kinetic model uncertainty quantification, propagation and minimization, Prog. Ener. Combust. Sci. 47 (2015) 1-31.

[12] H. N. Najm, B. J. Debusschere, Y. M. Marzouk, S. Widmer and O. P. Le Maître, Uncertainty quantification in chemical systems, Int. J. Numerical Methods in Eng. 85 (2011) 670-690.

[13] S. H. Lam and D. A. Goussis, The CSP method for simplifying kinetics, Int J. Chem. Kin. 26 (1994) 461–486.

[14] U. Maas and S. B. Pope, Simplifying chemical kinetics: Intrinsic low-dimensional manifolds in composition space, Combust. and Flame 88 (1992) 239–264.

[15] C. K. Law, C. J. Sung, H. Wang, and T. F. Lu, Development of comprehensive detailed and reduced reaction mechanisms for combustion modeling, AIAA Journal 41 (2003) 1629–1646.

[16] Z. C. Kramer, X. K. Gu, D. D. Y. Zhou, W. X. Li, R. T. Skodje, Following Molecules through Reactive Networks: Surface Catalyzed Decomposition of Methanol on Pd(111), Pt(111), and Ni(111), J. Phys. Chem. C 118 (2014) 12364-12383.

[17] S. R. Bai, D. Y. Zhou, M. J. Davis, R. T. Skodje, Sum Over Histories Representation of Chemical Kinetics, J. Phys. Chem. Lett. 6 (2015) 183-188.

[18] S. R. Bai, M. J. Davis, R. T. Skodje, Sum over Histories Representation for Kinetic Sensitivity Analysis: How Chemical Pathways Change when Reaction Rate Coefficients are Varied, J. Phys. Chem. A 119 (2015) 11039-11052.

[19] S. R. Bai, R. T. Skodje, Sum Over Histories Representation for Chemical Kinetics: A Quantitative Theory Based on Chemical Pathways, Int. Rev. Phys. Chem. 35 (2016) 539-567.

[20] S. R. Bai, R. T. Skodje, Simulating Chemical Kinetics Without Differential Equations: A Quantitative Theory Based on Chemical Pathways, J. Chem. Phys. Lett. 8 (2017) 3826.

[21] M. Alaghemandi, J. R. Green, Reactive symbol sequences for a model of hydrogen combustion, Phys. Chem. Chem. Phys. 18 (2016) 2810–2817.

[22] N. O. Temkin, A. V. Zeigarnik, D. G. Bonchev, Chemical Reaction Networks: A Graph-Theoretical Approach, CRC Press, Boca Raton, 1996.

[23] C. F. Goldsmith, W. H. Green, S. J. Klippenstein, J. Phys. Chem. A 116 (2012) 3325–3346.

- [24] S. S. Merchant, C. F. Goldsmith, A. G. Vandeputte, M. P. Burke, S. J. Klippenstein, W. H. Green, Combust. Flame 162 (2015) 3658-3673.
- [25] J. Zádor, C. A. Taatjes, R. X. Fernandes, Prog. Ener. Combust. Sci. 37 (2011) 371–421.
- [26] C. K. Westbrook, W. J. Pitz, O. Herbinet, H. J. Curran, E. J. Silke, A comprehensivedetailed chemical kinetic reaction mechanism for combustion of n-alkane hydrocarbons from n-octane to n-hexadecane, Combust. Flame 156 (2009) 181.
- [27] F. Battin-Leclerc, O. Herbinet, P. A. Glaude, R. Fournet, Z. Zhou, L. Deng, Experimental confirmation of the low-temperature oxidation scheme of alkanes, Angew. Chem. Int. Ed. 49 (2010) 3169.
- [28] H. J. Curran, P. Gaffuri, W. J. Pitz, C. K. Westbrook, A comprehensive modeling study of n-heptane oxidation, Combust. Flame 114 (1998) 149.
- [29] O. Welz, M. P. Burke, I. O. Antonov, C. F. Goldsmith, J. D. Savee, D. L. Osborn, C. A. Taajes, S. J. Klippenstein, L. Sheps, J. Phys. Chem. A 119 (2015) 7116–7129.
- [30] M. P. Burke, C. F. Goldsmith, S. J. Klippenstein, O. Welz, H. Huang, I. V. Antovov, J. D. Savee, D. L. Osborn, J. Zador, C. A. Tajjes, L. Sheps, J. Phys. Chem. A 119 (2015) 7095.
- [31] J. F. Griffiths, Prog. Energy Combust. Sci. 21 (1995) 25.
- [32] M. Bodenstein, Z. Phys. Chem. 85 (1913) 329.
- [33] C. N. Hinshelwood, H. W. Thompson, The kinetics of the combination of hydrogen and oxygen, Proc. Roy. Soc. London A 118 (1928) 170-183.
- [34] N. Semenoff, Chemical Kinetics and Chain Reaction, Oxford University Press, Oxford, 1935.
- [35]G. Li, H. Rabitz, A general analysis of exact lumping in chemical kinetics. Chem. Eng. Sci. 44 (1989) 1413–1430.
- [36] A. S. Tomlin, T. Turanyi, M. J. Pilling, Mathematical tools for the construction, investigation and reduction of combustion mechanisms. In: Pilling, M.J., Hancock, G. (eds.) Low-temperature Combustion and Autoignition. Comprehensive Chemical Kinetics 35 (1997), 293–437.
- [37] E. Ranzi, T. Faravelli, P. Gaffuri, A. Sogaro, Low-temperature combustion: automatic generation of primary oxidation reactions and lumping procedures. Combust. Flame 102, (1995) 179–192.
- [38] J. Austin, On the explicit versus family solution of the fully diurnal photochemical equations of the stratosphere, J. Geophys. Res. Atmos. 96(D7) (1991) 12941–12974.
- [39] J. A. Christiansen, The Elucidation of Reaction Mechanisms by the Method of Intermediates in Quasi-Stationary Concentrations, Adv. Catalysis 5 (1953) 311-353.
- [40] E. L. King, C. A. Altman, Schematic Method of Deriving the Rate Laws for Enzyme-Catalyzed Reactions, J. Phys. Chem. 60 (1956) 1375-1378.
- [41] I. Fishtik, C. A. Callaghan, R. Datta, Reaction Route Graphs. I. Theory and Algorithm J. Phys. Chem. B 108 (2004) 5671-5682.
- [42] H. Feng, B. Han, J. Wang, Dominant Kinetic Paths of Complex Systems: Gene Networks, J. Phys. Chem. Lett. 1 (2010) 1836-1840.
- [43] R. Lehmann, An algorithm for the determination of all significant pathways in chemical reaction systems, J. Atmos. Chem. 47 (2004) 45-78.
- [44] K. Y. He, Kaiyuan, M. G. Ierapetritou, I. P. Androulakis, A graph-based approach to developing adaptive representations of complex reaction mechanisms, Combust. Flame 155 (2008) 585-604.
- [45] B. Bollobas, Modern Graph Theory, Springer Verlag, Berlin, 1998.
- [46] C. H. Schilling, D. Letscher, B. O. Palsson, Theory for the Systemic Definition of Metabolic Pathways and their use in Interpreting Metabolic Function from a Pathway-Oriented Perspective, J. Theor. Biol. 203 (2000) 229-248.
- [47] T. Lu, C. K. Law, Linear time reduction of large kinetic mechanisms with directed relation graph: n-Heptane and iso-octane, Combust. and Flame 144 (2006) 24-36.
- [48] T. Lu, C. K. Law, A directed relation graph method for mechanism reduction, Proc. Combust. Inst. 30 (2005) 1333-1341.
- [49] R. Gacia-Domenech, J. Galvez, J. V. Julian-Ortiz, L. Pogliani, Some New Trends in Chemical Graph Theory, Chem. Rev. 108 (2008) 1127-1169.
- [50] J. Revel, J. C. Boettner, M. Cathonnet, J. S. Bachman, Derivation of a Global Chemical Mechanism for Methane Ignition and Combustion, J. Chim. Phys. 91 (1994) 365-382.
- [51] D. T. Gillespie, A General Method for Numerically Simulating the Stochastic Time Evolution of Coupled Chemical Reactions, J. Comp. Phys. 22 (1976) 403-434.

- [52] D. T. Gillespie, A. Hellander, L. R. Petzold, Perspective:Stochastic Algorithms for Chemical Kinetics, J. Chem. Phys. 138 (2013) 170901.
- [53] M. Bastian, S. Heymann, M. Jacomy, Gephi: an open source software for exploring and manipulating networks. International AAAI Conference on Weblogs and Social Media (2009).
- [54] V. D. Blondel, J.-L. Guillaume, R. Lambiotte, E. Lefebvre, Fast unfolding of communities in large networks, p10008 J. Stat. Mech. (2008).
- [55] C. Demetrescu, I. Finocchi, G. I. Italiano, Dynamic Graph Algorithms in Handbook of Graph Theory, CRC Press, Boca, 2004.
- [56] D. E. Kaufman, R. L. Smith, Fastest Paths in Time-Dependent Networks for Intelligent Vehicle-Highway Systems Application, IVHS 1 (1993) 1-11.
- [57] F. Harrary, G. Gupta, Dynamic Graph Models. Math. Comput. Modelling 25 (1997) 79-87.
- [58] R. Atkinson, D. L. Baulch, R. A. Cox, J. N. Crowley, R. F. Hampson, R. G. Hynes, M. E. Jenkin, M. J. Rossi and J. Troe, Evaluated Kinetic and Photochemical Data for Atmospheric Chemistry: Volume II Gas Phase Reactions of Organic Species, Atmos. Chem. Phys. 6 (2006) 3625-4055 and references within.
- [59] M. T. Raventos-Duran, C. J. Percival, M. R. McGillen, P. D. Hamer, D. E. Shallcross, Kinetics and Branching Ratio Studies of the Reaction of $C_2H_5O_2 + HO_2$ using Chemical Ionization Mass Spectrometry, Phys. Chem. Chem. Phys. 9 (2007) 4338-4348.
- [60] A. C. Noell, L. S. Alconcel, D. J. Robichaud, M. Okumura, S. P. Sander, Near-Infrared Kinetic Spectroscopy of the HO₂ and C₂H₅O₂ Self-Reactions and Cross Reactions, J. Phys. Chem. A 114 (2010) 6983-6995.
- [61] H. Adachi and N. Basco, Spectra of Propylperoxy Radicals and Rate Constants for Mutual Interaction, Int. J. Chem. Kinet. 14 (1982), 1125-1138.